Molecular organization in the twist-bend nematic phase by resonant X-ray scattering at the Se K-edge and by SAXS, WAXS and GIXRD

W. D. Stevenson[1], Z. Ahmed[2], X. B. Zeng[1,*], C. Welch[2], G. Ungar[1,3] and G. H. Mehl[2,*]

[1] Department of Materials Science and Engineering, University of Sheffield, Sheffield S1 3JD, UK
[2] Department of Chemistry, University of Hull, Hull HU6 7RX, UK
[3] Department of Physics, Zhejiang Sci-Tech University, Hangzhou 310018, China

Supporting Information

Table of Contents

1.0 – Synthesis of DTSe 2
1.1. – Chemical Analysis -Spectroscopic data for compounds 1-4 5
2.0 – Miscibility of DTC5C7 and DTSe 20
3.0 – DSC Analysis of DTC5C7, DTSe and Mixtures 21
4.0 – X-ray Scattering of Se45 22
4.1 – X-ray Fluorescence of Se45 22
4.2 – Resonant Scattering Features of Se45 22
4.3 – Non-resonant Scattering Features of Se45 23
5.0 – Geometric Calculations of the Helical Structure 25
5.1 – Tilt Angle of the Mesogens 25
5.2 - BendAngle of the Dimers 26
5.3 – Twist Angle of the Dimers 26
5.4 – Tilt Angle of the Dimers 27
6.0 – Molecular Modelling 28

1.0 – Synthesis of DTSe

The Se-labelled compound DTSe was synthesised for resonant X-ray scattering (RXS) investigation using the four stage process shown diagrammatically in figure S1 below. The details of each step are also provided in the appropriate sub section. Spectroscopic infomration is listed subsequently.

Starting reagents and solvents were purchased from Fischer, Sigma Aldrich, Acros Organics and Fluorochem and used without further purification. Boronic acids were purchased from Kingston chemicals and were also used without further purification.

The structures after purification were confirmed by ^{1}H and ^{13}C nuclear magnetic resonance spectroscopy. The experiments were performed with a Joel JNM-ECP 400 MHz FT-NMR. The chemical shifts reported in this section are relative to tetramethylsilane used as an internal standard and coupling constants *J* are reported in Hertz (Hz). ^{1}H experiments were performed at 400 MHz, ^{13}C at 100 MHz and ^{19}F 376 MHz.

Low resolution electron ionisation (EI), electro-spray (ES), chemical ionisation (CI), matrix assisted laser deposition ionisation (MALDI) and high resolution mass spectrometry (HRMS) were obtained via the EPSRC National Mass Spectrometry Service Centre at Swansea University, Wales.

The purity of the final compounds was confirmed by high performance liquid chromatography. The HPLC setup consisted of Gilson 321 pump, Agilent/HP1100 detector with a Phenomex LUNA 18(2) reverse phase C18 column. The column dimensions are 250 mm x 4.6 mm, 5 µm particles and 100 Å pore size.

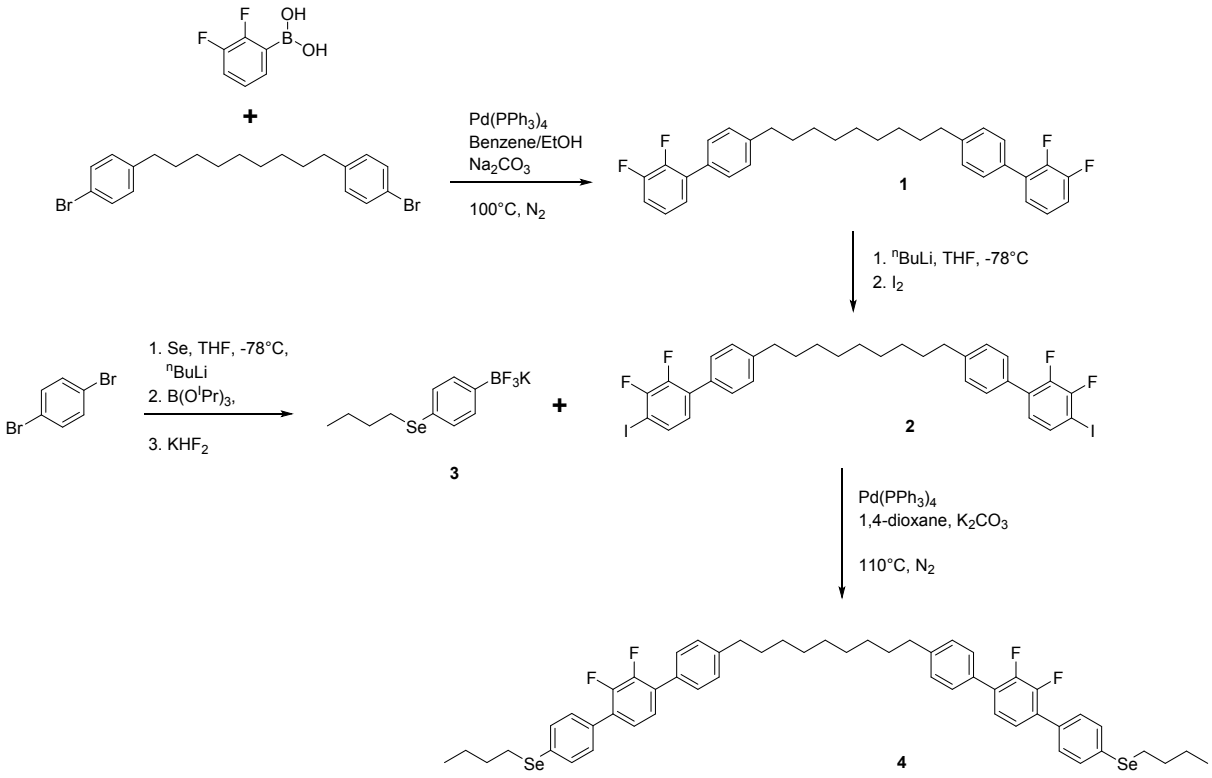

Figure S1 – The Four step Synthesis of the Se-labelled compound DTSe (Compound 4).

Compound 1: 1,9-bis(2',3'-difluoro-[1,1'-biphenyl]-4-yl)nonane

A stirred solution of 1,9-bis(4-bromophenyl)nonane (0.82g, 1.9mmol) and $Pd(PPh_3)_4$ (79mg, 0.07mmol, 4mol%) in benzene (15mL) were added to a solution of sodium carbonate (2M, 15mL) under

nitrogen atmosphere. Nitrogen gas was bubbled through the resulting two-phase mixture for 10 minutes and then a solution of (2,3-difluorophenyl) boronic acid (0.77g, 4.9mmol) in ethanol (15mL) was added. The reaction was heated under reflux conditions to 100°C for 15 hours. After cooling to ambient temperature, diethyl ether (150mL) and water (100mL) were added to the mixture. The separated organics were then washed with water (2x100mL) and dried over $MgSO_4$(s). After removal of the dessicant by filtration, the solvent was concentrated in vacuo and the product isolated by column chromatography (Silica gel, eluent: hexane/CH_2Cl_2, 9:1). Yield 0.79g, 84%.

δ_H(400MHz; CD_2Cl_2) δ 7.48-7.40 (m, 4H), 7.27 (d, ^{3}J=8.4Hz, 4H), 7.23-7.06 (m, 6H), 2.64 (t, ^{3}J=7.8Hz, 4H), 1.63 (q, J = 7.4 Hz, 4H), 1.43-1.25 (m, 10H)

δ_C(100MHz; CD_2Cl_2) δ 151.58 (dd, ^{1}J(C-F) = 247 Hz, ^{2}J(C-F) = 13.8 Hz), 148.41 (dd, ^{1}J(C-F) = 248 Hz, ^{2}J(C-F) = 13.1 Hz), 143.75 (s), 132.31 (d, J(C-F) = 2.3 Hz), 131.69 (d, J(C-F) = 10.0 Hz), 129.16 (d, J(C-F) = 3.1 Hz), 129.06 (s), 125.78-125.72 (m), 124.54 (dd, J(C-F) = 7.7 Hz, 4.6 Hz), 116.07 (d, J(C-F) = 17.7 Hz), 36.05 (s), 31.88 (s), 29.94 (s), 29.91 (s), 29.76 (s)

δ_F(376MHz; CD_2Cl_2) -139.09 (dt, ^{3}J(F-F) = 20.8 Hz, ^{4}J(F-H) = 6.9 Hz), -144.75 (dd, ^{3}J(F-F) = 20.8 Hz, ^{4}J(F-H) = 4.6 Hz)

Compound 2: 1,9-bis(2',3'-difluoro-4'-iodo-[1,1'-biphenyl]-4-yl)nonane.

Compound (**1**) (0.67g, 1.3 mmol) was dissolved in anhydrous THF (15 mL) under a dry N_2 atmosphere and the solution was cooled to -78°C. ^{n}BuLi (1.6M, 1.83 mL, 2.9 mmol) was added dropwise and (after the addition) the reaction was left to stir for 1 hour at -78°C. A solution of iodine (0.74g, 2.9 mmol) in anhydrous THF (15mL) was then added. The reaction was stirred for 16hrs, slowly rising to ambient temperature. Water (100mL) and diethyl ether (100mL) were added to separate the organics, which were then washed successively with brine (50mL) and $Na_2S_2O_3$(aq) (saturated solution, 100 mL). The organic layer was separated and dried over $MgSO_4$(s). After removal of the dessicant by filtration the solvents were concentrated to leave a yellow residue which quickly solidified. The pure product was obtained by recrystallization from ethanol.

δ_H(400MHz; CD_2Cl_2) 7.54 (ddd, ^{3}J = 8.4 Hz, ^{4}J(H-F) = 5.7 Hz, ^{5}J(H-F) = 2.0 Hz, 2H), 7.42 (dd, ^{3}J = 8.3 Hz, ^{4}J =1.8 Hz, 4H), 7.26 (d, ^{3}J = 8.4 Hz, 4H), 7.03-6.96 (m, 2H), 2.63 (t, J = 7.8 Hz, 4H), 1.69-1.57 (m, 4H), 1.39-1.27 (m, 10H)

δ_C(100MHz; CD_2Cl_2) 151.47 (dd, ^{1}J(C-F) = 244.5 Hz, ^{2}J(C-F) = 14.6 Hz), 147.84 (dd, ^{1}J(C-F) = 252.9 Hz, ^{2}J(C-F) = 14.6 Hz), 144.12 (s), 133.72 (d, J(C-F) = 3.8 Hz), 131.97 (d, J(C-F) = 10.8 Hz), 131.53 (br s), 129.12 (s), 128.96 (d, J(C-F) = 3.1 Hz), 126.89 (m), 80.23 (d, ^{2}J(C-F) = 23.1 Hz), 35.69 (s), 31.77 (s), 29.83 (s), 29.80 (s), 29.65 (s)

δ_F(376MHz; CD_2Cl_2) -117.92 (dd, ^{3}J(F-F) = 20.8 Hz, ^{4}J(F-H) = 4.6 Hz), -140.06 (dd, ^{3}J(F-F) = 20.8 Hz, ^{4}J(F-H) = 6.9 Hz)

MS (EI) *m/z* 756.0 $(M)^+$
HRMS : calculated for $C_{33}H_{30}F_4I_2$: 756.0373, found 756.0373

Compound 3: Potassium 4-(Butylselanyl)phenyltrifluoroborate.

A solution of 1,4-dibromobenzene (2.36g, 10 mmol) and selenium powder (0.79 g, 10 mmol) in anhydrous THF (60 mL) was cooled to -78°C in a nitrogen atmosphere. ^{n}BuLi (2.2 M in cyclohexane, 4.5 mL, 10 mmol) was

added dropwise and the reaction was warmed to 0°C over a period of 30 minutes. After the reaction mixture was clear, triisopropyl borate (1.88 g, 2.31 mL, 10 mmol) was added (at 0°C) and the reaction mixture was re-cooled to -78°C. ^{n}BuLi (2.2 M in cyclohexane, 4.5 mL, 10 mmol) was then slowly added. After 10 minutes at -78°C the temperature was raised to -10°C and the reaction was stirred at this temperature for 40 minutes. The reaction mixture was quenched with KHF_2(aq) (1N, 25 mL, 25 mmol) and then warmed to room temperature. After stirring for 15 minutes, the suspension was concentrated and the residual solid was dissolved in dry acetone (80 mL). The insoluble salts were filtered off and the resulting organic solution was concentrated to leave a solid. This was dissolved in acetone (70 mL) and diethyl ether (70 mL) and precipitated to produce an off-white solid, 1.64g, 51%

δ_H(400MHz; $(CD_3)_2CO$) 7.41 (d, ^3J = 7.7 Hz, 2H), 7.26 (d, ^3J = 7.6 Hz, 2H), 2.82 (t, ^3J = 7.3 Hz, 2H), 1.62 (m, 2H), 1.40 (m, 2H), 0.87 (t, ^3J = 7.3 Hz, 3H)

δ_C(100MHz; $(CD_3)_2CO$) 133.42, 132.07, 126.78, 33.17, 27.88, 23.46, 13.82

δ_F(376MHz; $(CD_3)_2CO$) -142.54

δ_B(128 MHz; $(CD_3)_2CO$) 2.69

MS (NSI) *m/z* 274.03 $(M\text{-}K)^-$
HRMS : calculated for $C_{10}H_{13}{}^{10}BF_3{}^{74}Se$: 274.0329, found 274.0335

Compound 4: 1,9-bis(4''-(butylselanyl)-2',3'-difluoro-[1,1':4',1''-terphenyl]-4-yl)nonane.

$Pd(PPh_3)_4$ (28 mg, 0.02mmol, 6mol%) and K_2CO_3 (0.33 g, 2.4 mmol) were added to a mixture of (**2**) (0.3g, 0.4 mmol) and (**3**) (0.25g, 0.8 mmol) dissolved in 1,4-dioxane (32 mL) and water (8 mL). Nitrogen gas was bubbled through the mixture for 10 minutes and the reaction was subsequently heated to 110°C for 15 hours under an N_2 atmosphere. After cooling to ambient temperature, the organics were separated by adding diethyl ether (150mL) and water (100mL). The organics were washed with water (2x100mL) and dried over $MgSO_4$(s). After removal of the dessicant by filtration, the solvent was concentrated in vacuo and the product isolated by column chromatography (Silica gel, eluent: hexane/CH_2Cl_2, 8:2). Yield 0.25 g, 68%.

δ_H(400MHz; CD_2Cl_2) 7.58-7.54 (m, 4H), 7.52-7.46 (m, 8H), 7.30 (d, ^3J = 8.2 Hz, 4H), 7.28-7.26 (m, 4H), 2.99 (t, ^3J = 7.3 Hz, 4H), 2.67 (t, ^3J = 7.6 Hz, 4H), 1.77-1.61 (m, 8H), 1.51-1.29 (m, 14H), 0.93 (t, ^3J = 7.3 Hz, 6H)

δ_C(100MHz; CD_2Cl_2) 148.93 (dd, ^1J = 249.8Hz, ^2J = 15.4Hz), 148.75 (dd, ^1J = 249.8 Hz, ^2J = 15.4 Hz), 143.85 (s), 133.04 (s), 132.20 (s), 132.00 (s), 130.22 (dd, J(C-F) = 8.5 Hz, 2.3 Hz), 129.68 (s), 129.30-129.19 (m), 129.12 (s), 129.04 (br s), 125.24-125.17 (m), 124.97-124.90 (m), 36.03 (s), 32.64 (s), 31.85 (s), 29.86 (s), 29.83 (s), 29.69 (s), 27.67 (s), 23.39 (s), 13.73 (s)

δ_F(376MHz; CD_2Cl_2) -143.92 (s)

MS (EI) *m/z* 928.1 $(M)^+$

1.1. – Chemical Analysis -Spectroscopic data for compounds 1-4

Compound 1

^{1}H-NMR data for compound 1

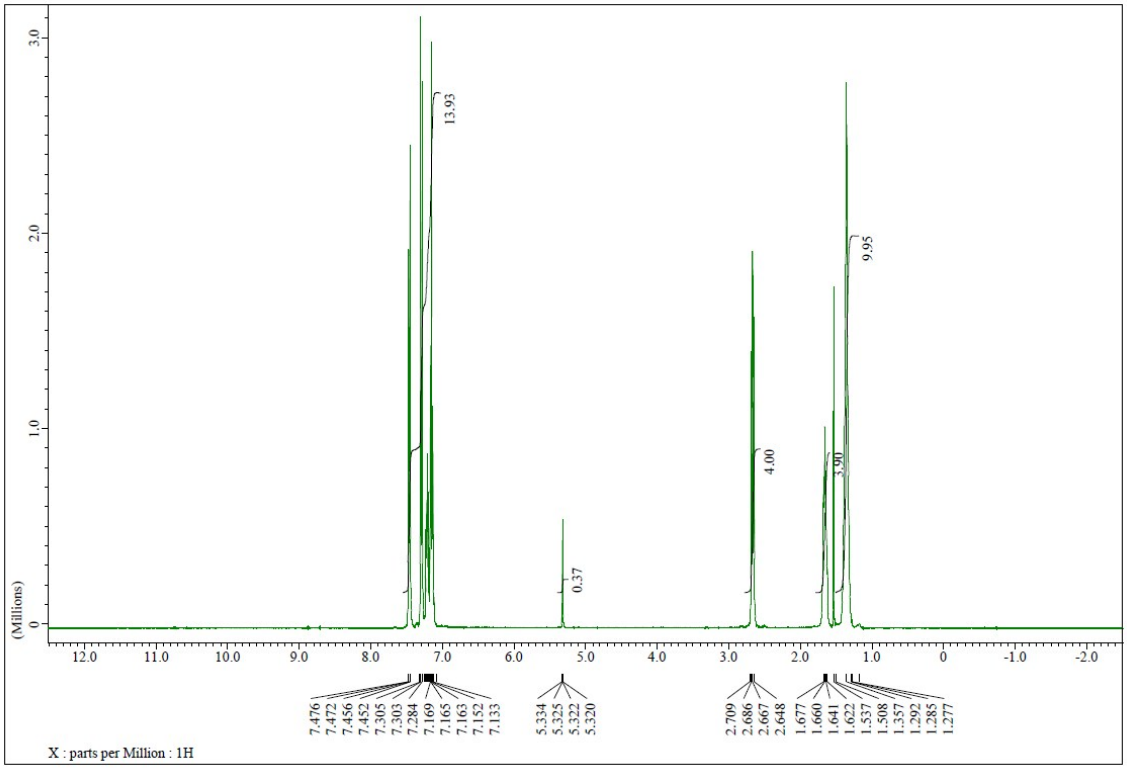

^{13}C- NMR data for compound 1

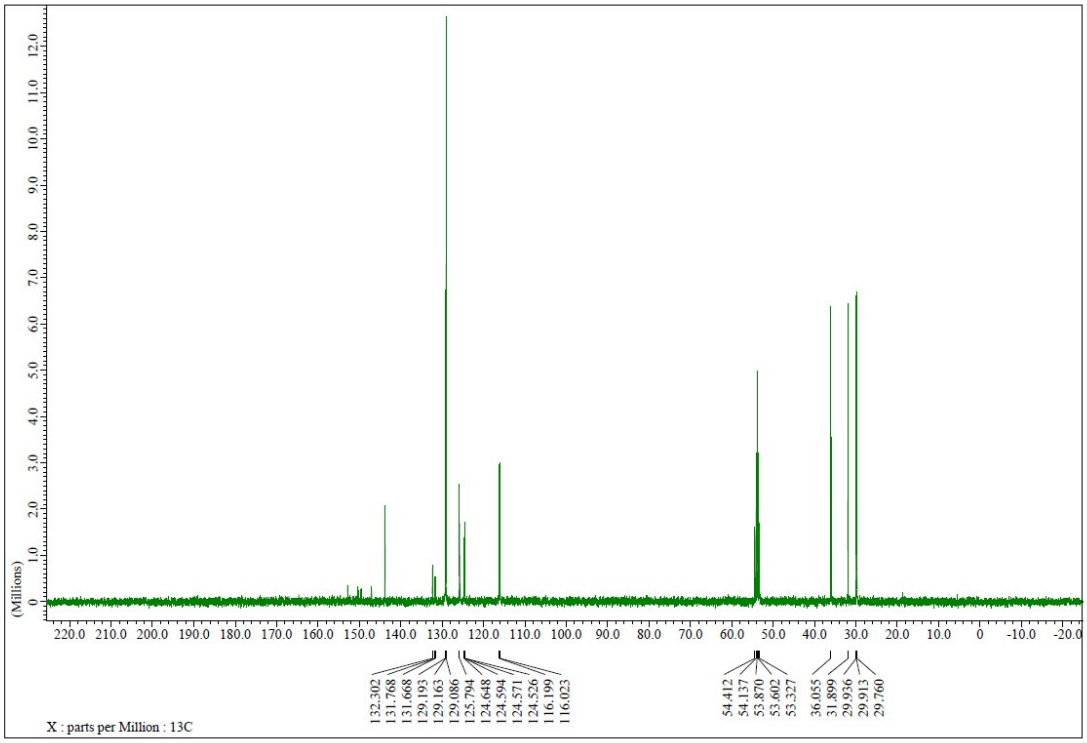

Compound 2

^{1}H-NMR data for compound 2

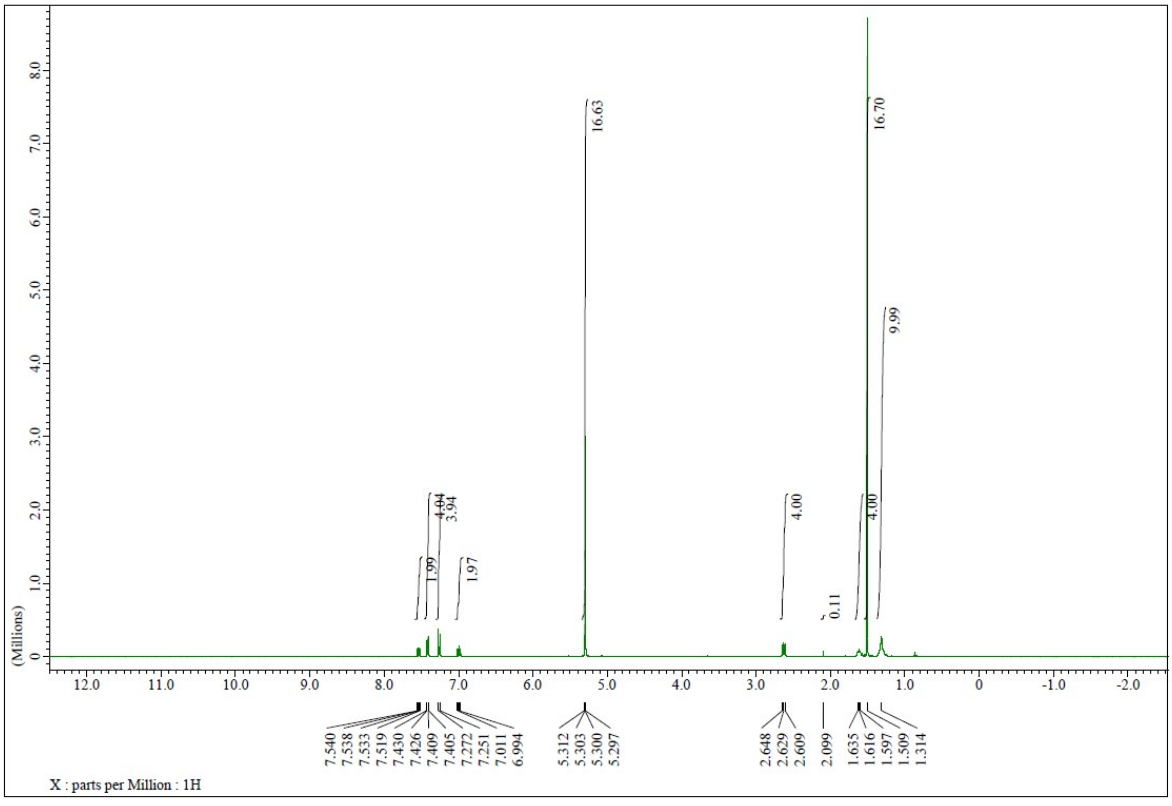

^{13}C- NMR data for compound 2

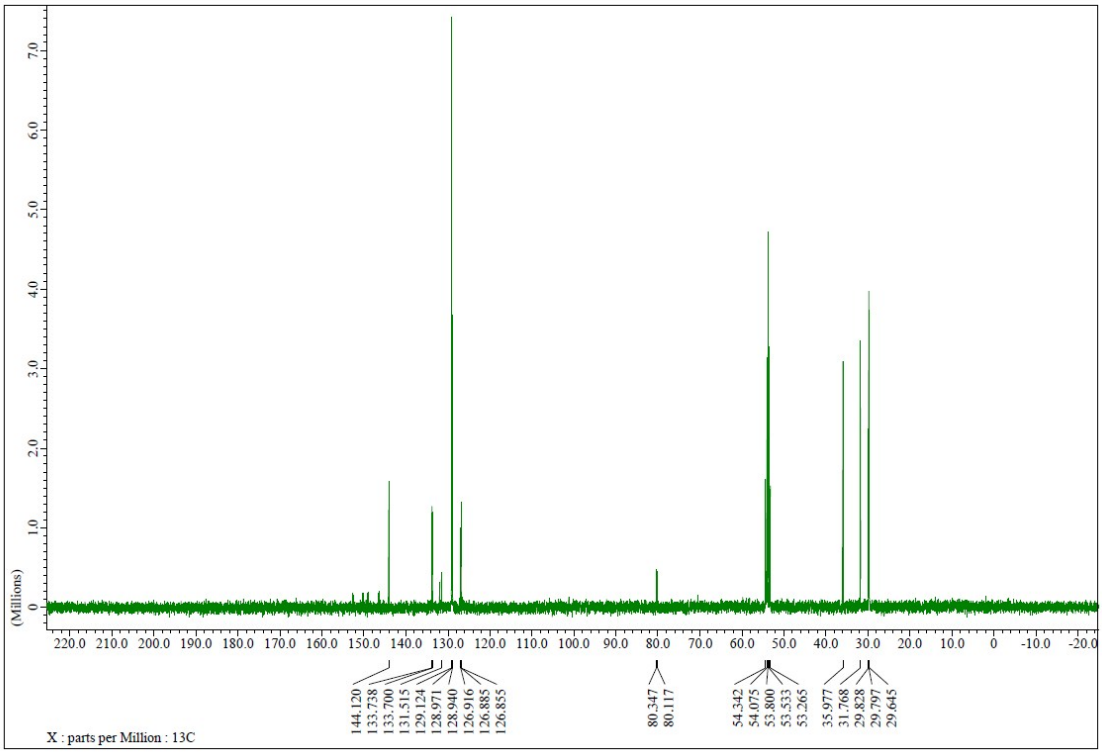

^{19}F –NMR data for compound 2

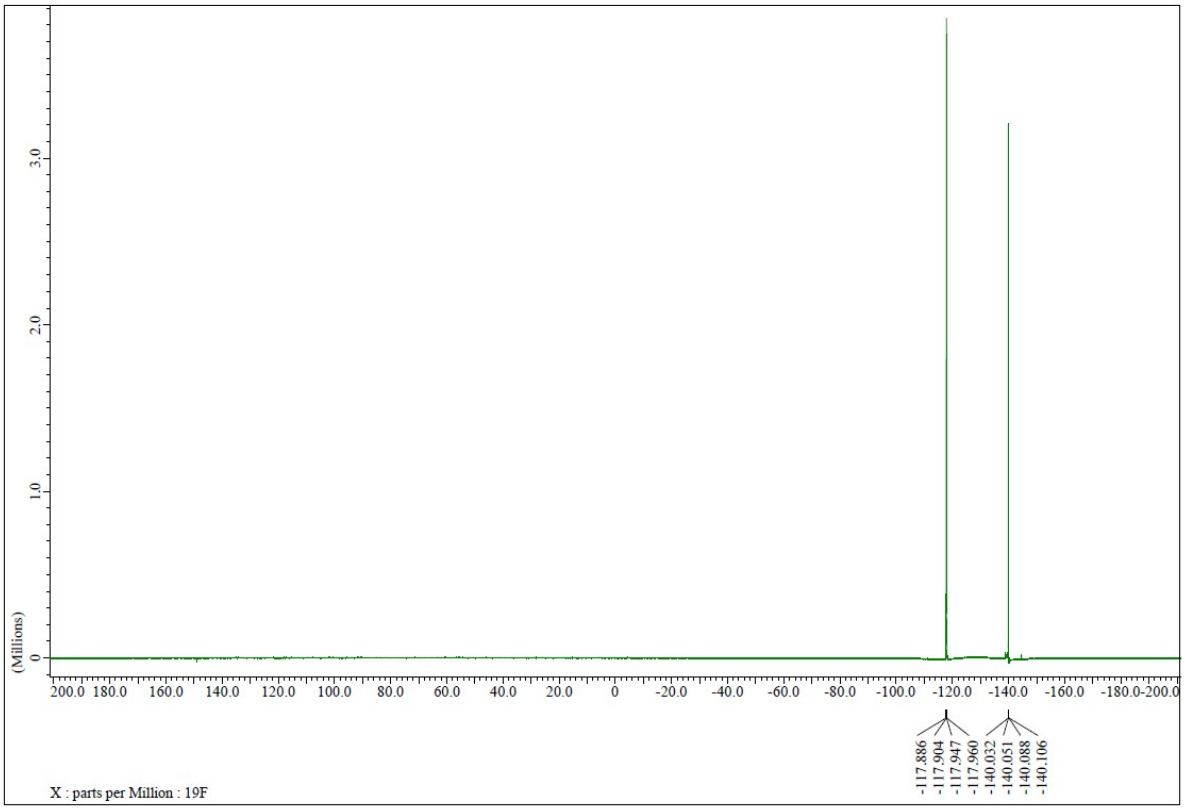

High Resolution Mass spectroscopy data for compound 2

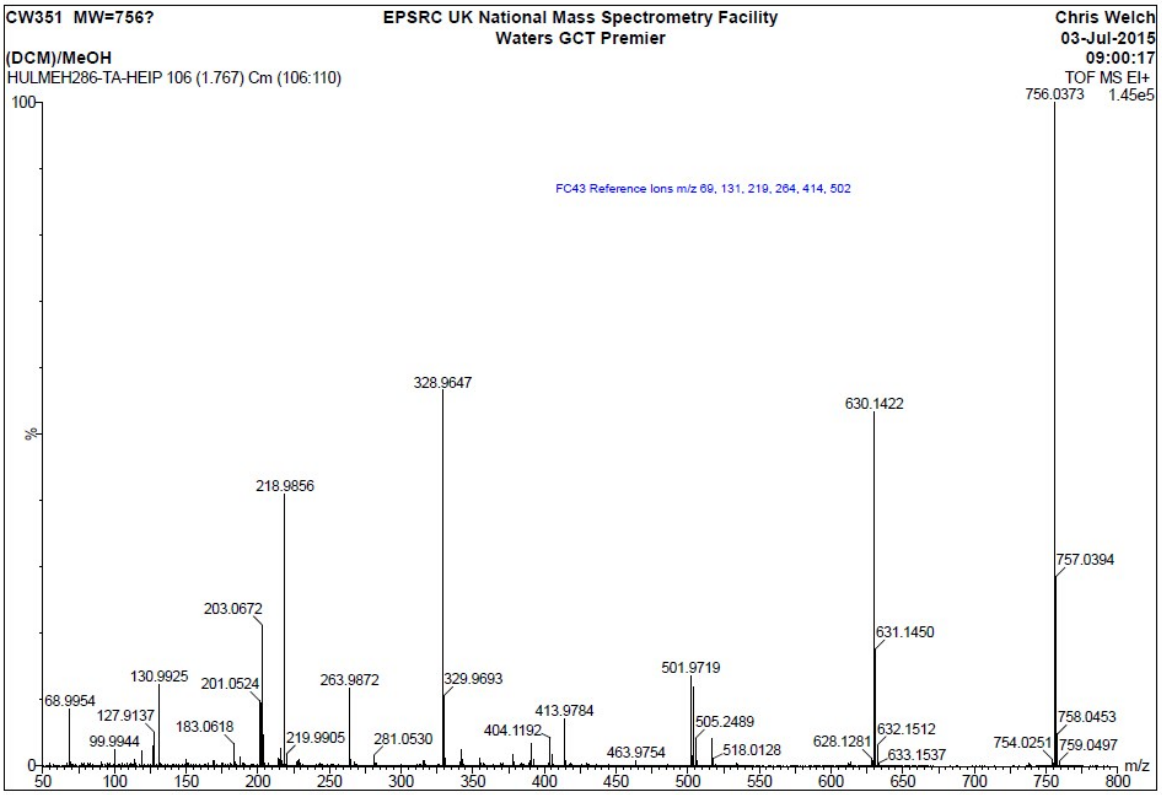
CW351 MW=756?
EPSRC UK National Mass Spectrometry Facility
Waters GCT Premier
Chris Welch
03-Jul-2015
09:00:17
(DCM)/MeOH
HULMEH286-TA-HEIP 106 (1.767) Cm (106:110)
TOF MS EI+
1.45e5
FC43 Reference Ions m/z 69, 131, 219, 264, 414, 502
756.0373
328.9647
630.1422
218.9856
757.0394
203.0672
631.1450
130.9925
201.0524
263.9872
329.9693
501.9719
68.9954
127.9137
183.0618
413.9784
505.2489
758.0453
99.9944
219.9905
281.0530
404.1192
632.1512
628.1281
754.0251
759.0497
463.9754
518.0128
633.1537
%
m/z

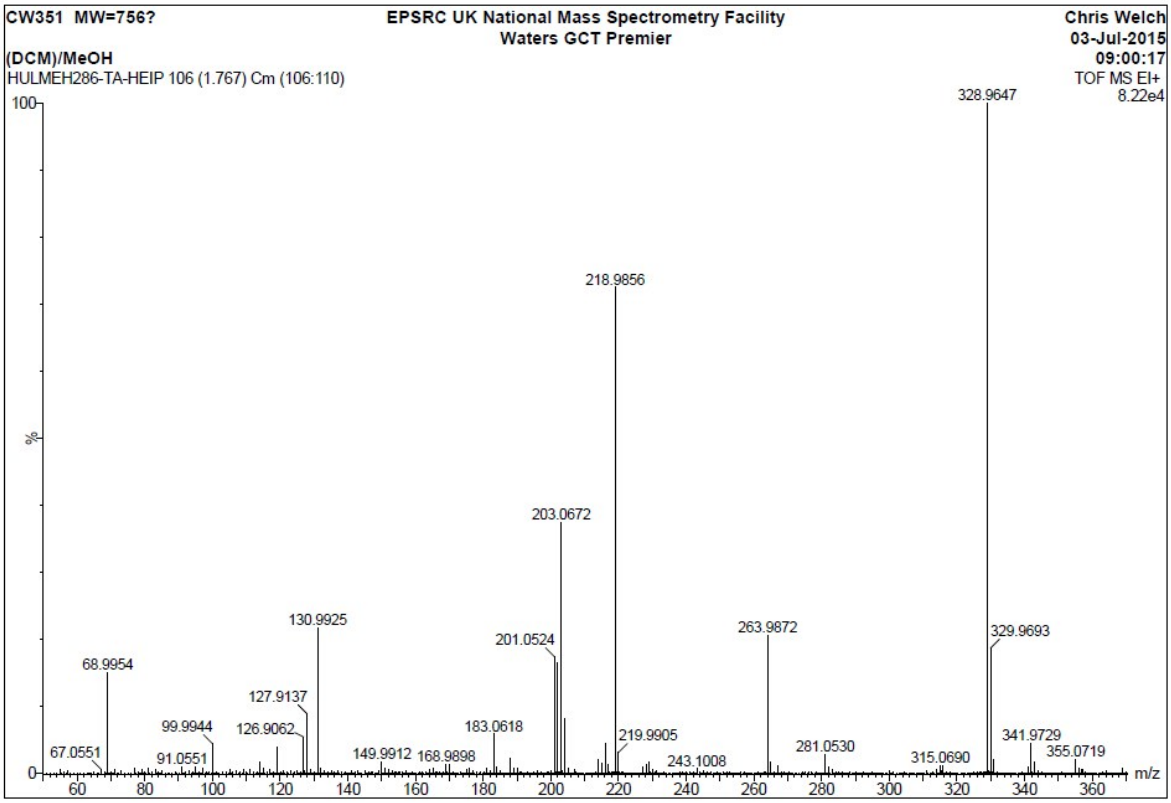
CW351 MW=756?
EPSRC UK National Mass Spectrometry Facility
Waters GCT Premier
Chris Welch
03-Jul-2015
09:00:17
(DCM)/MeOH
HULMEH286-TA-HEIP 106 (1.767) Cm (106:110)
TOF MS EI+
8.22e4
328.9647
218.9856
203.0672
130.9925
263.9872
329.9693
201.0524
68.9954
127.9137
99.9944
126.9062
183.0618
219.9905
281.0530
341.9729
355.0719
67.0551
91.0551
149.9912
168.9898
243.1008
315.0690
%
m/z

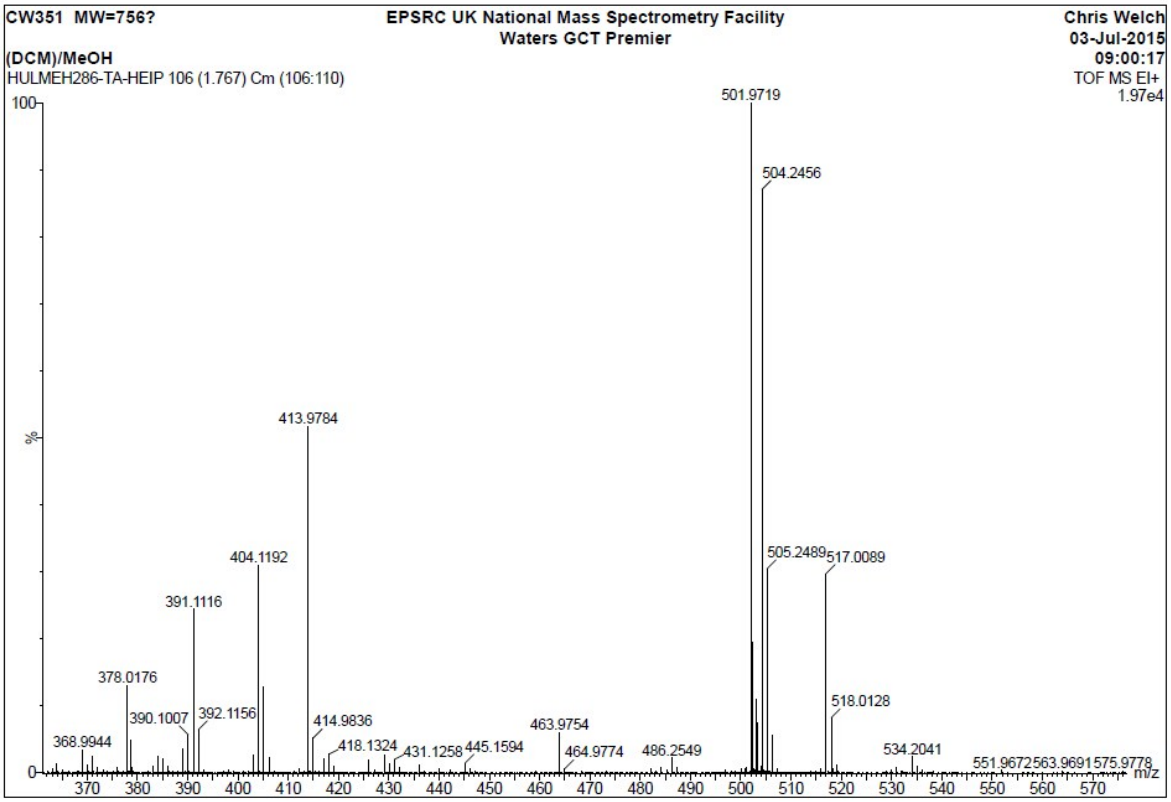

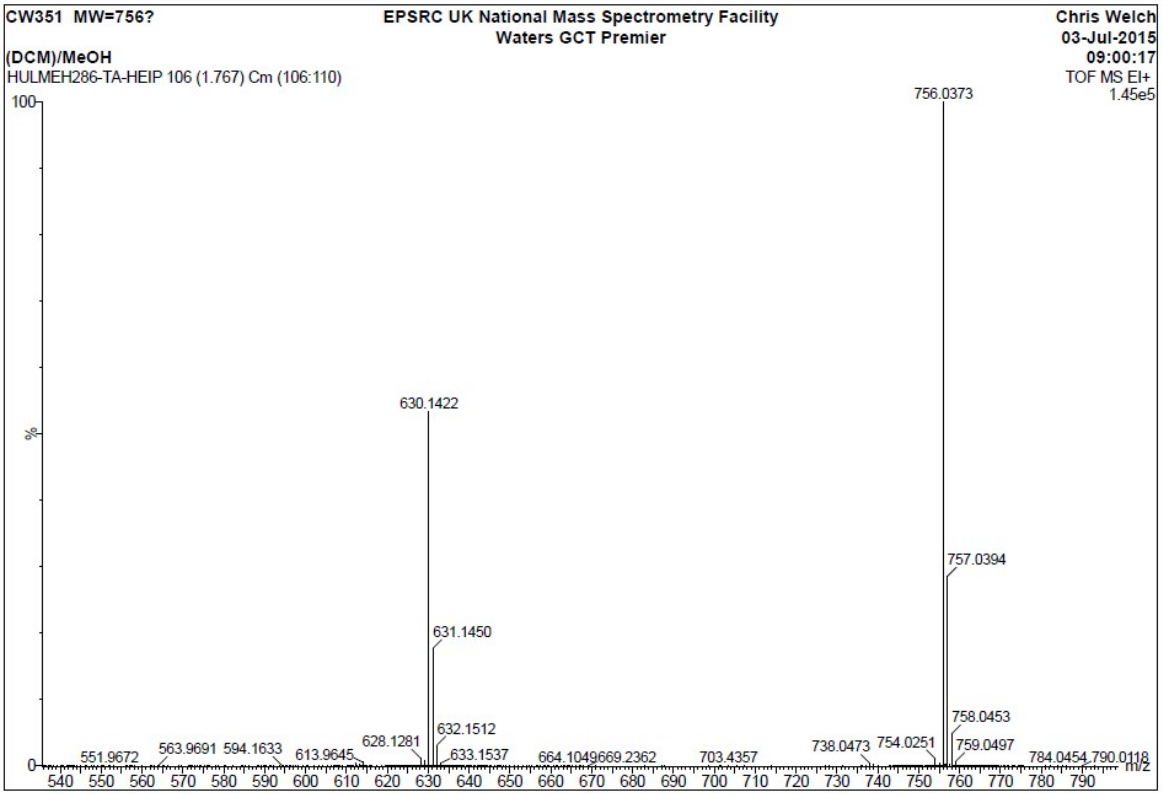

Comparison of theoretical and experimental isotope profile for compound 2

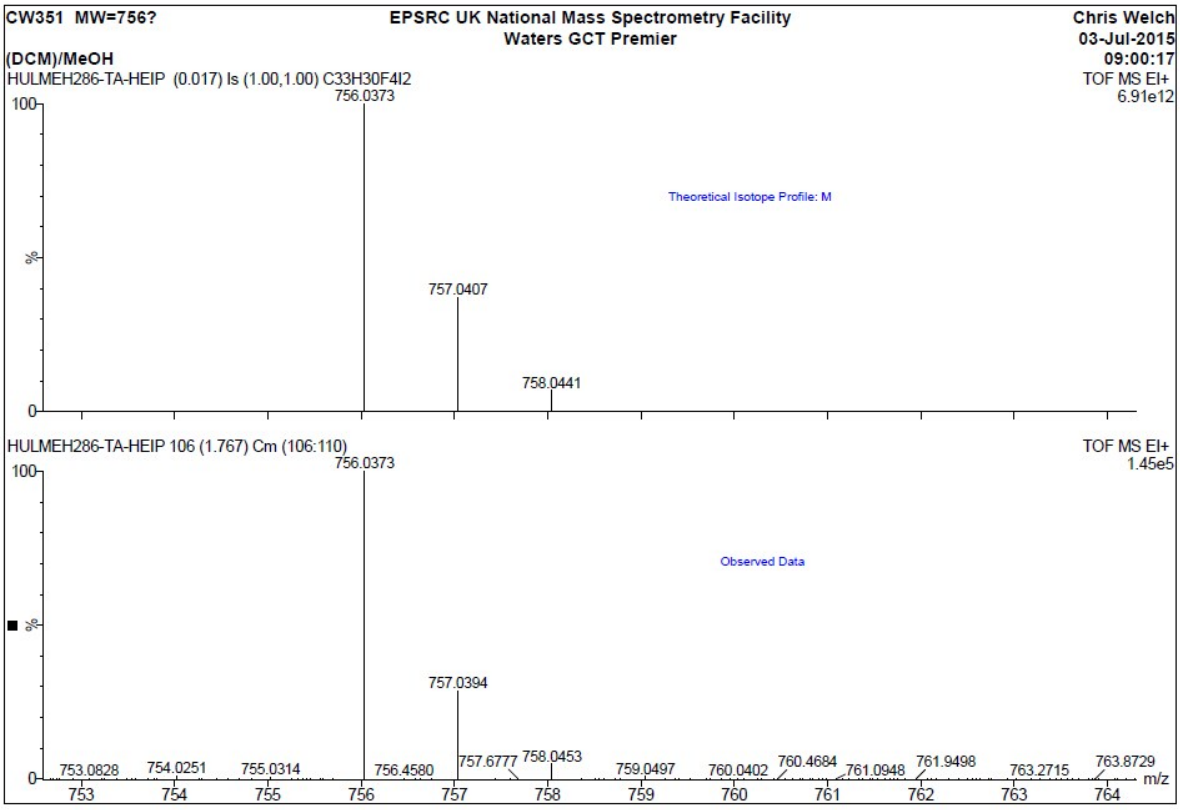

Compound 3

^{1}H-NMR data for compound 3

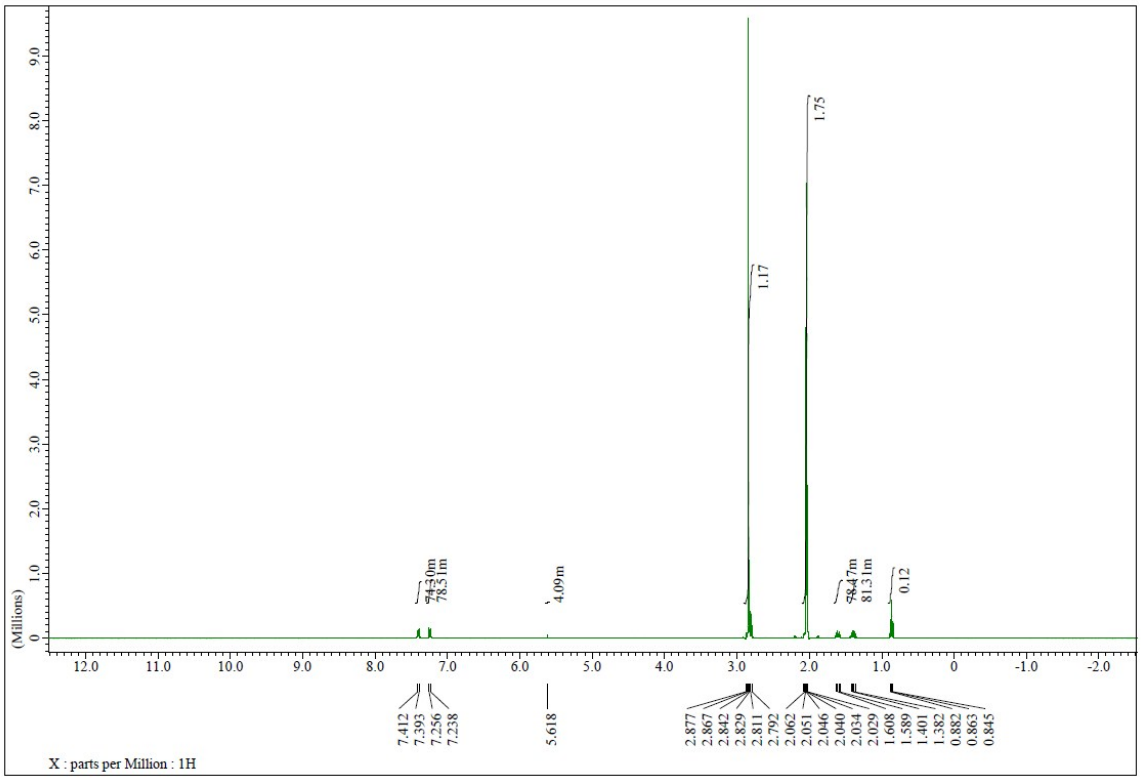

^{13}C- NMR data for compound 3

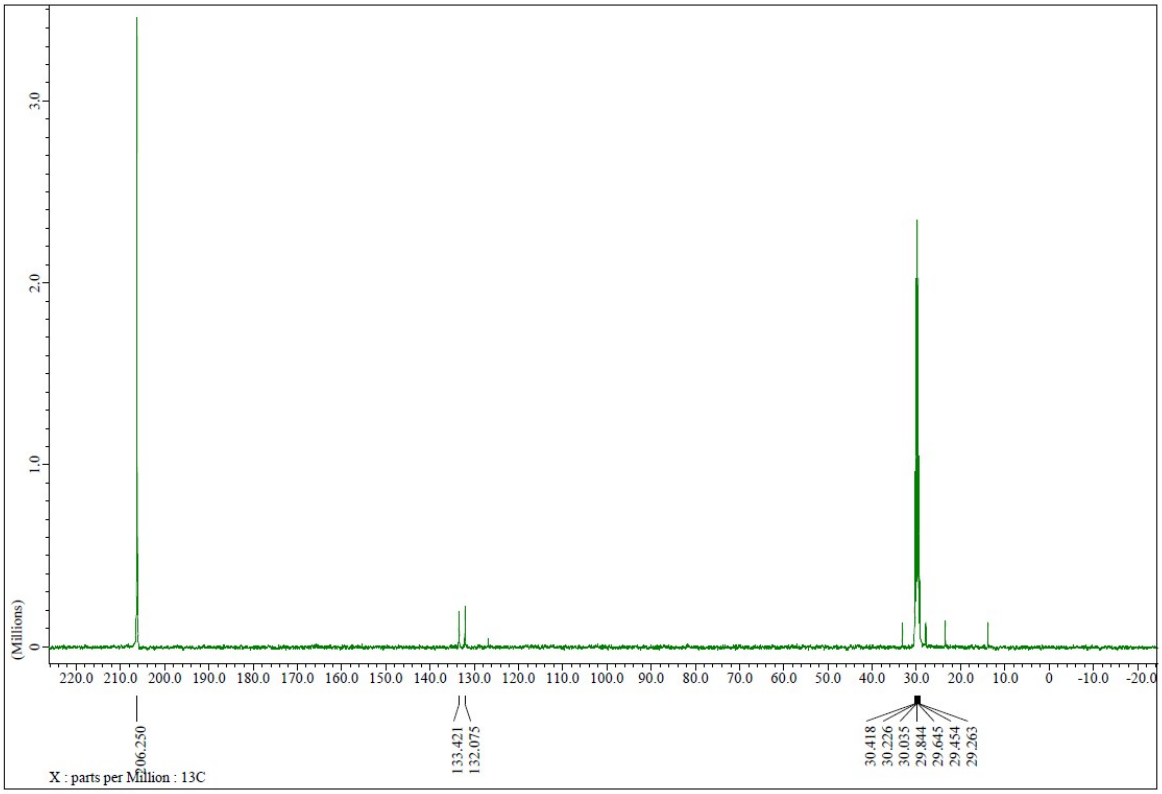

^{11}B- NMR data for compound 3

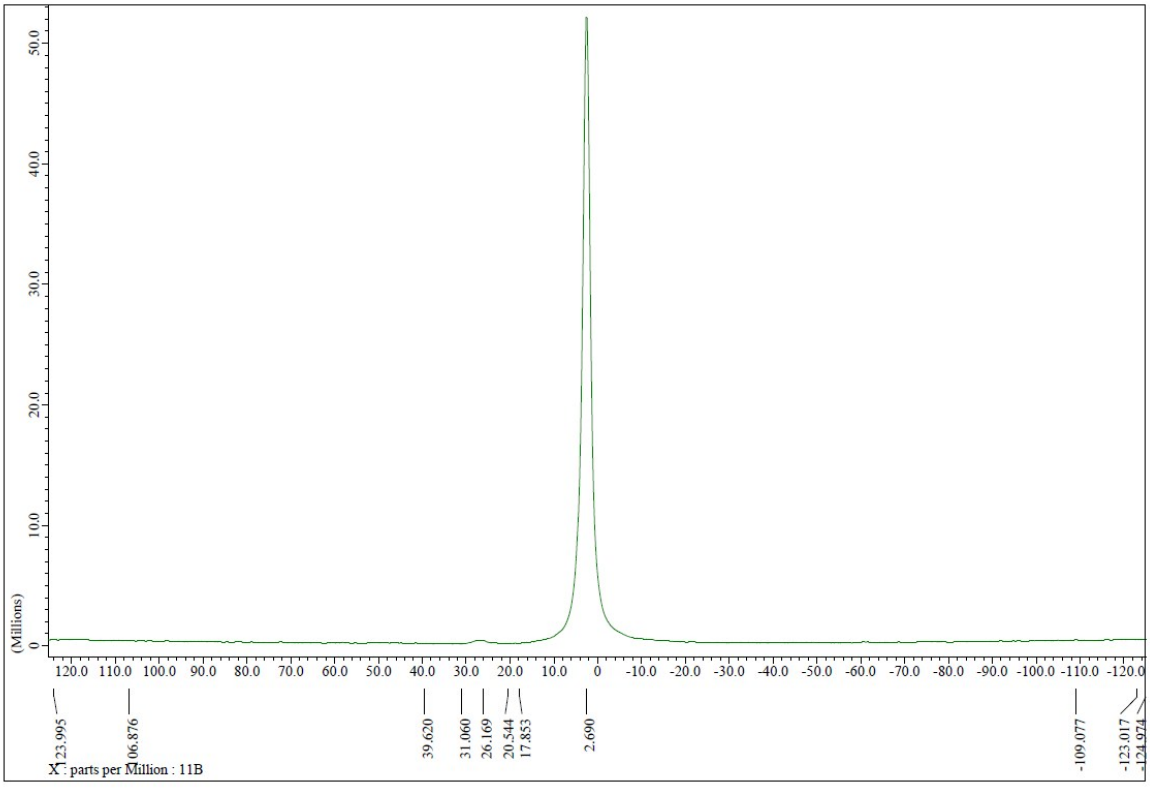

^{19}F –NMR data for compound 3

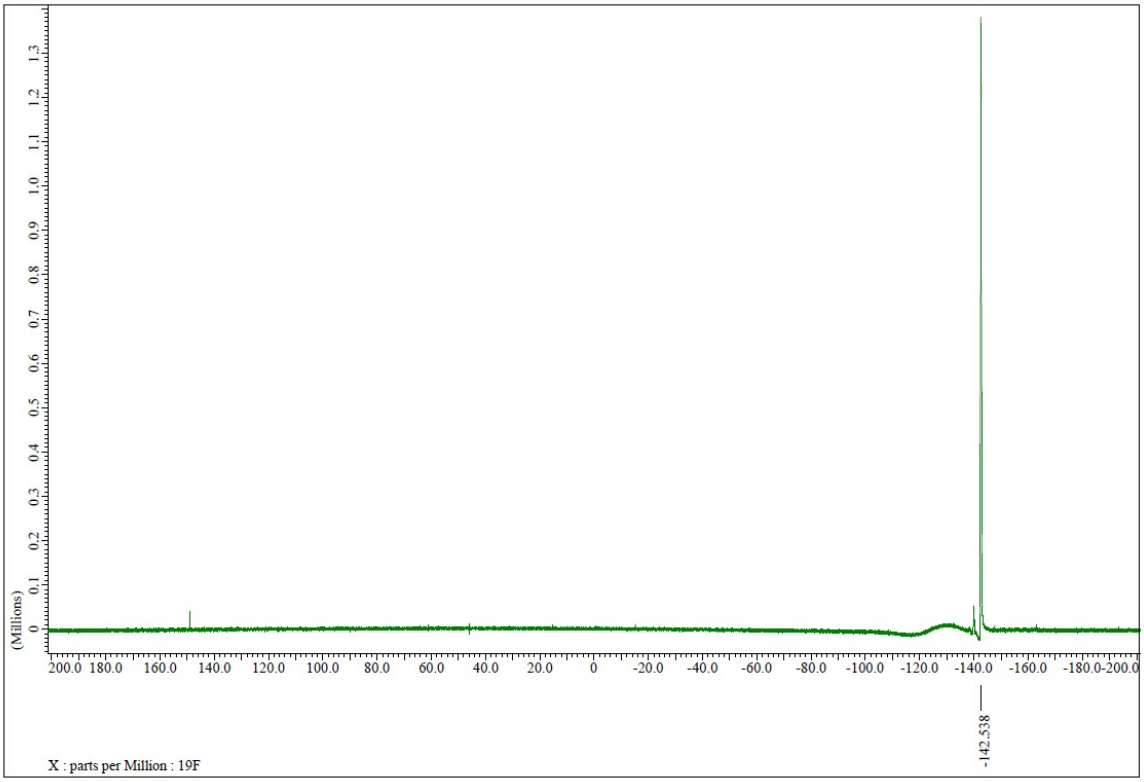

High Resolution Mass spectroscopy data for compound 3

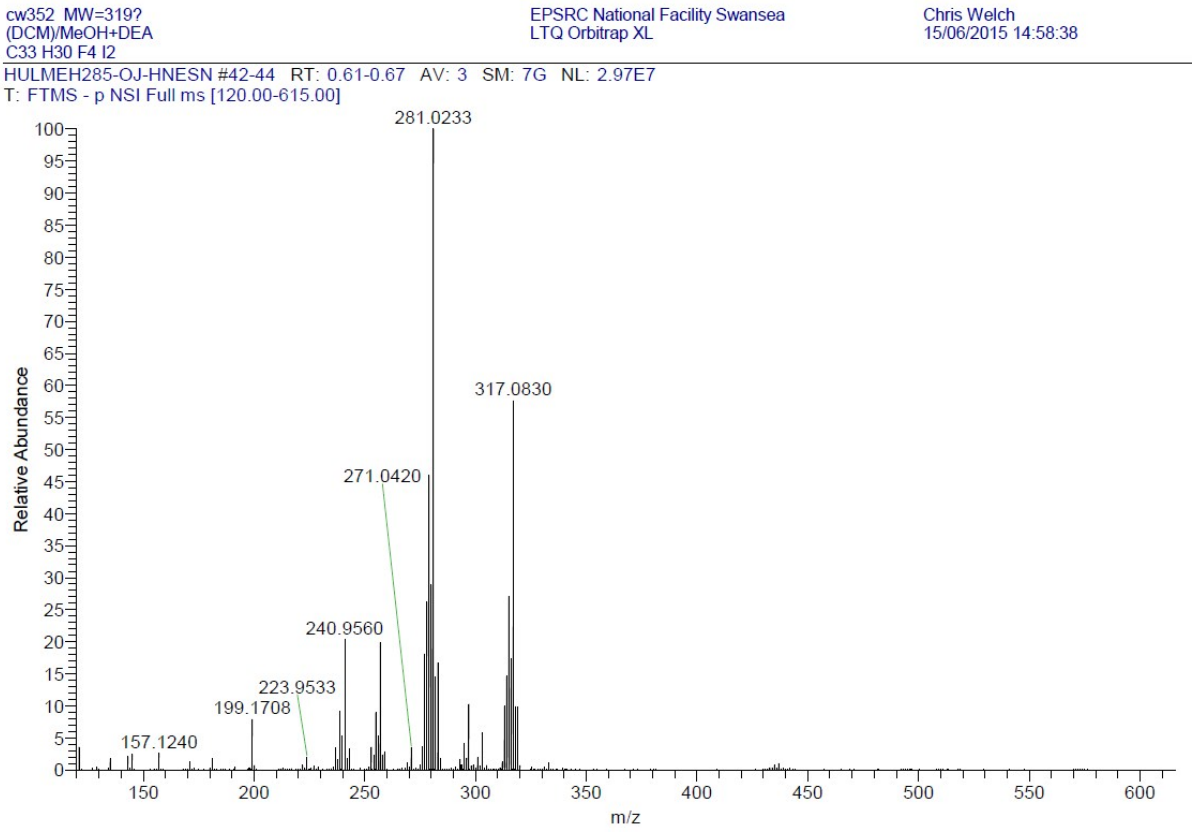

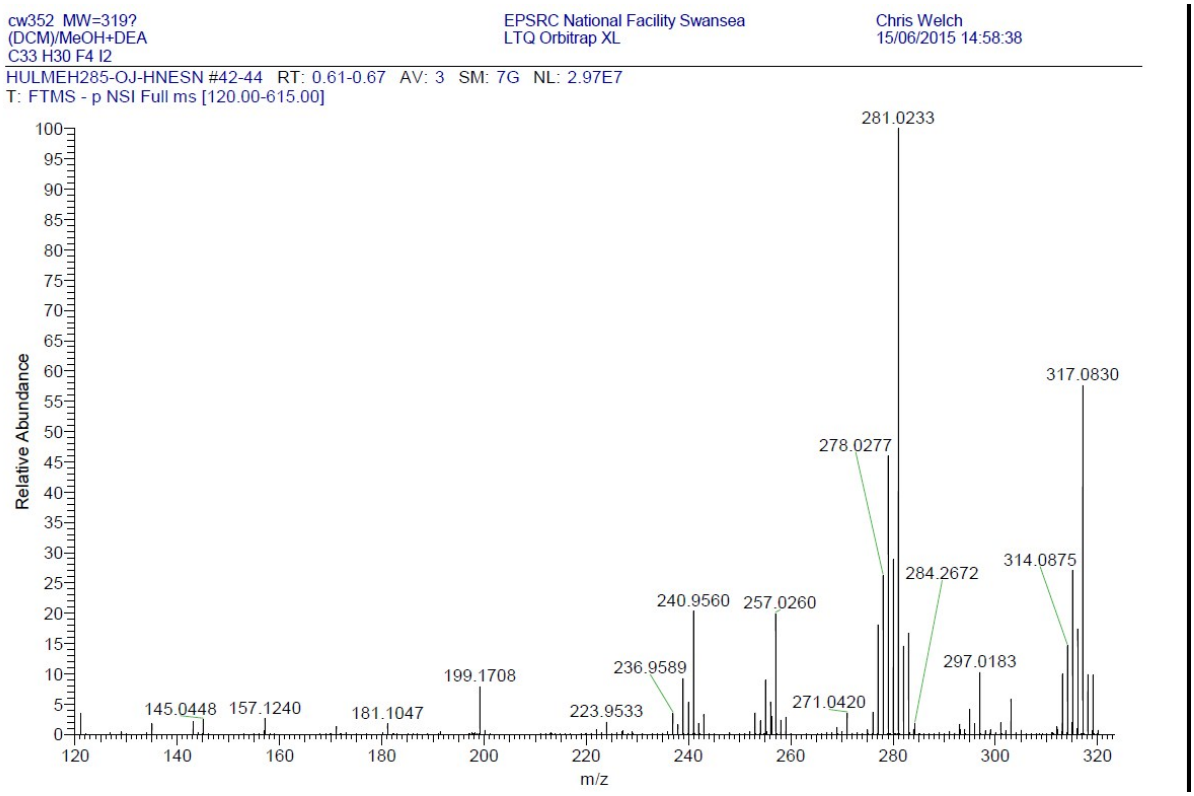

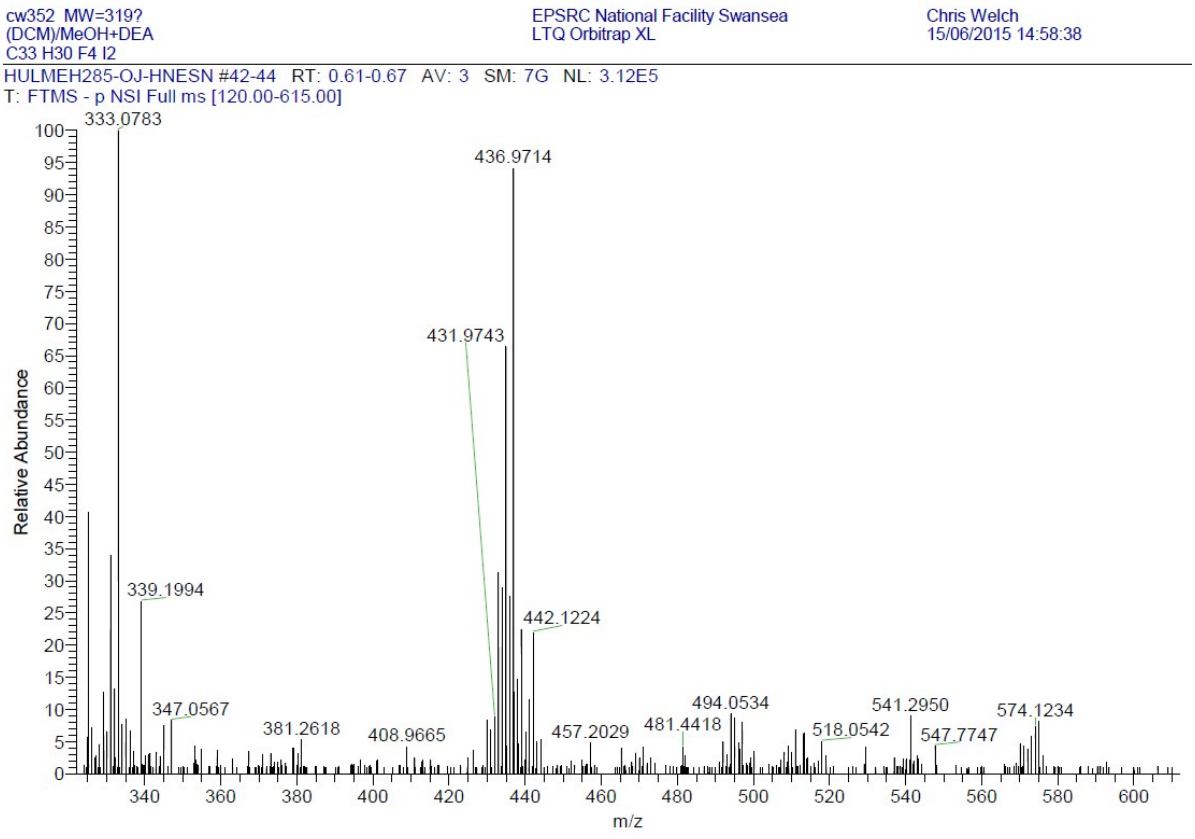

Comparison of theoretical and experimental isotope profile for compound 3

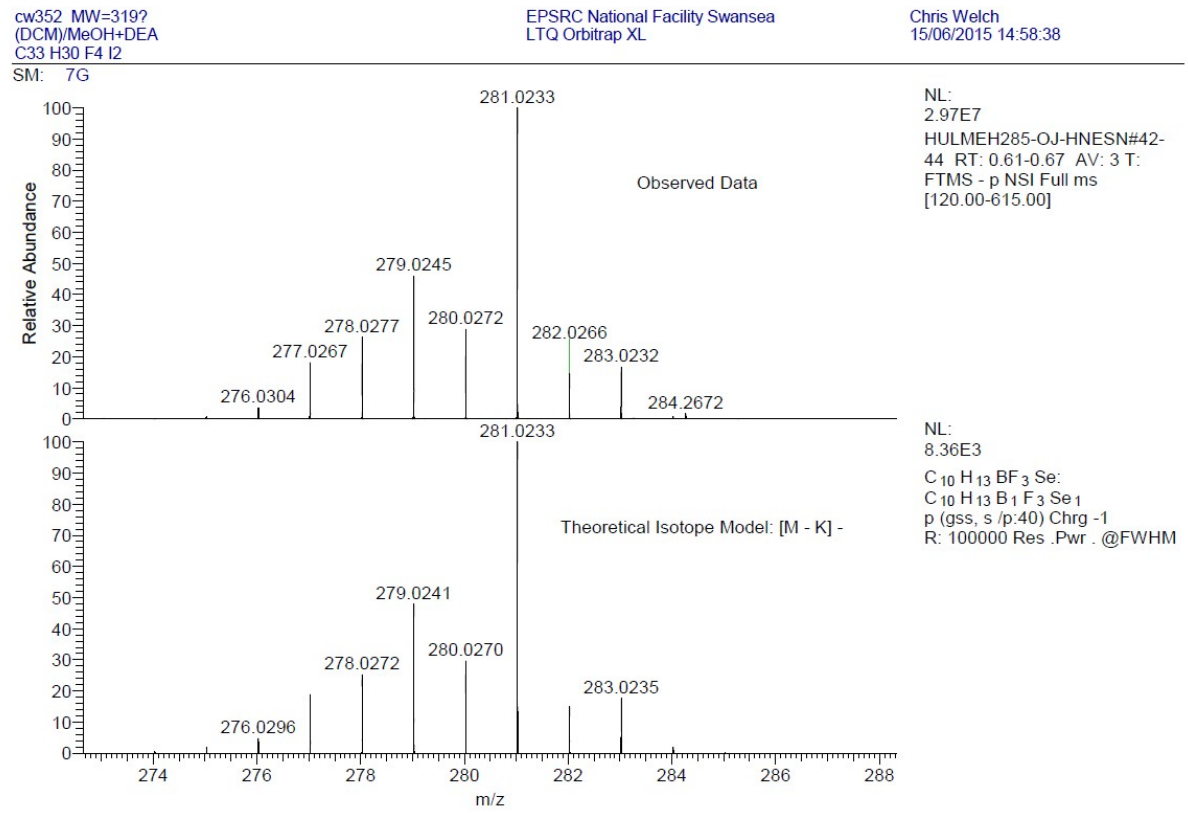

Compound 4

^{1}H-NMR data for compound 4

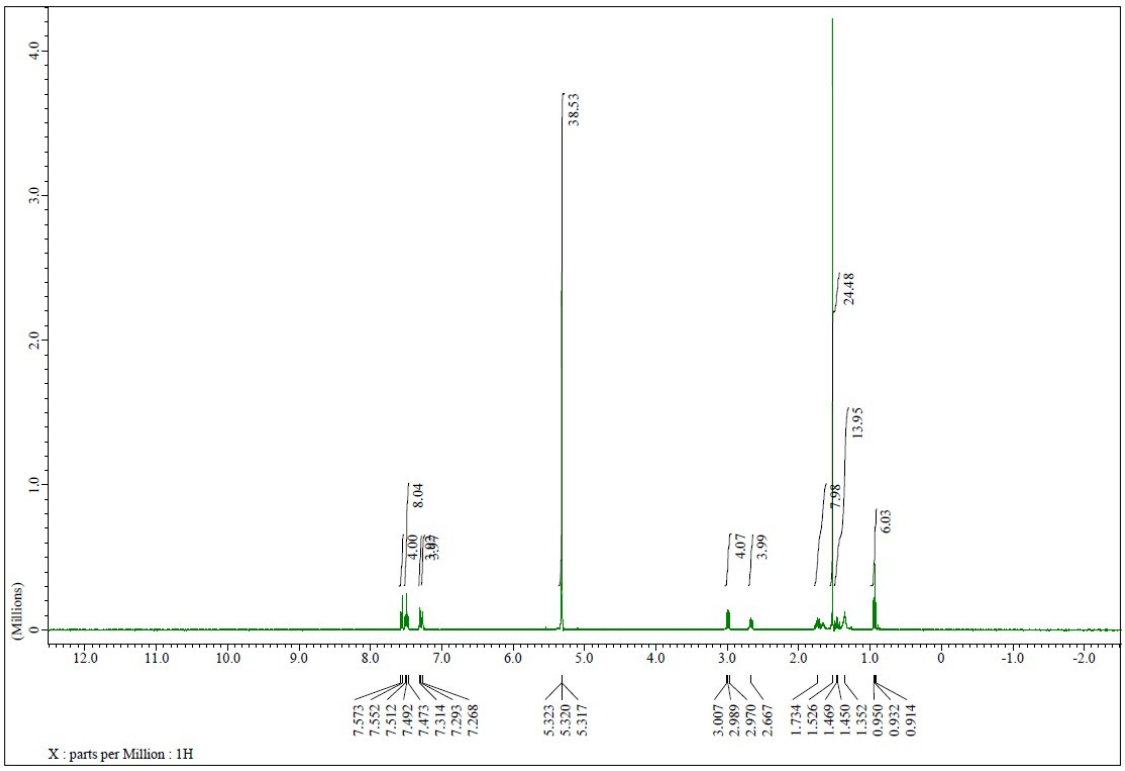

^{13}C- NMR data for compound 4

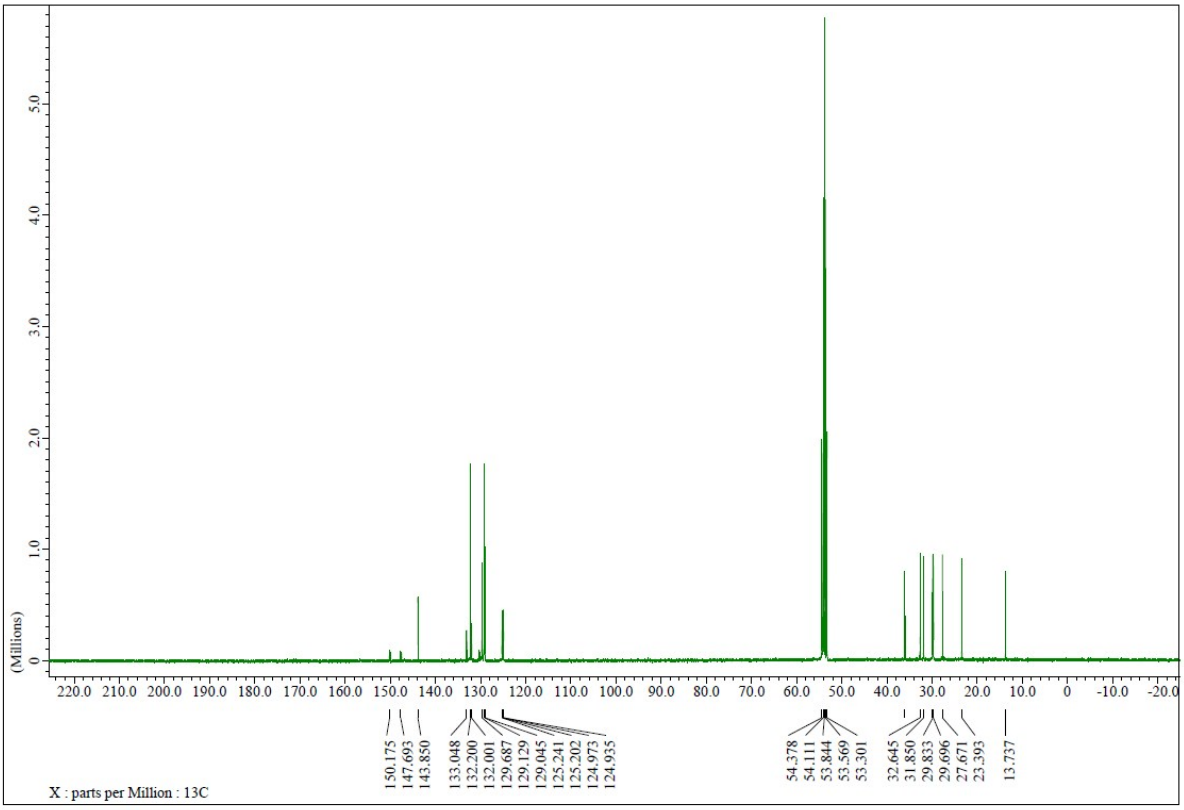

^{19}F –NMR data for compound 4

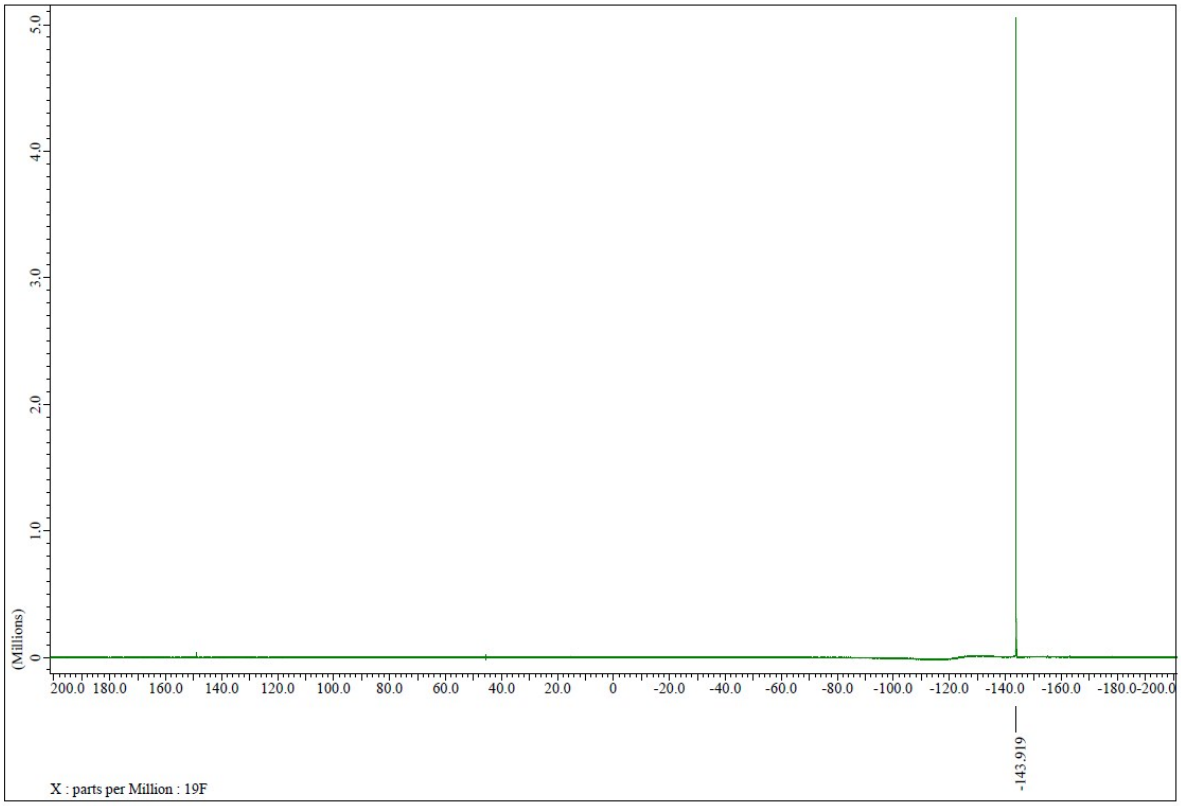

High Resolution Mass spectroscopy data for compound 4

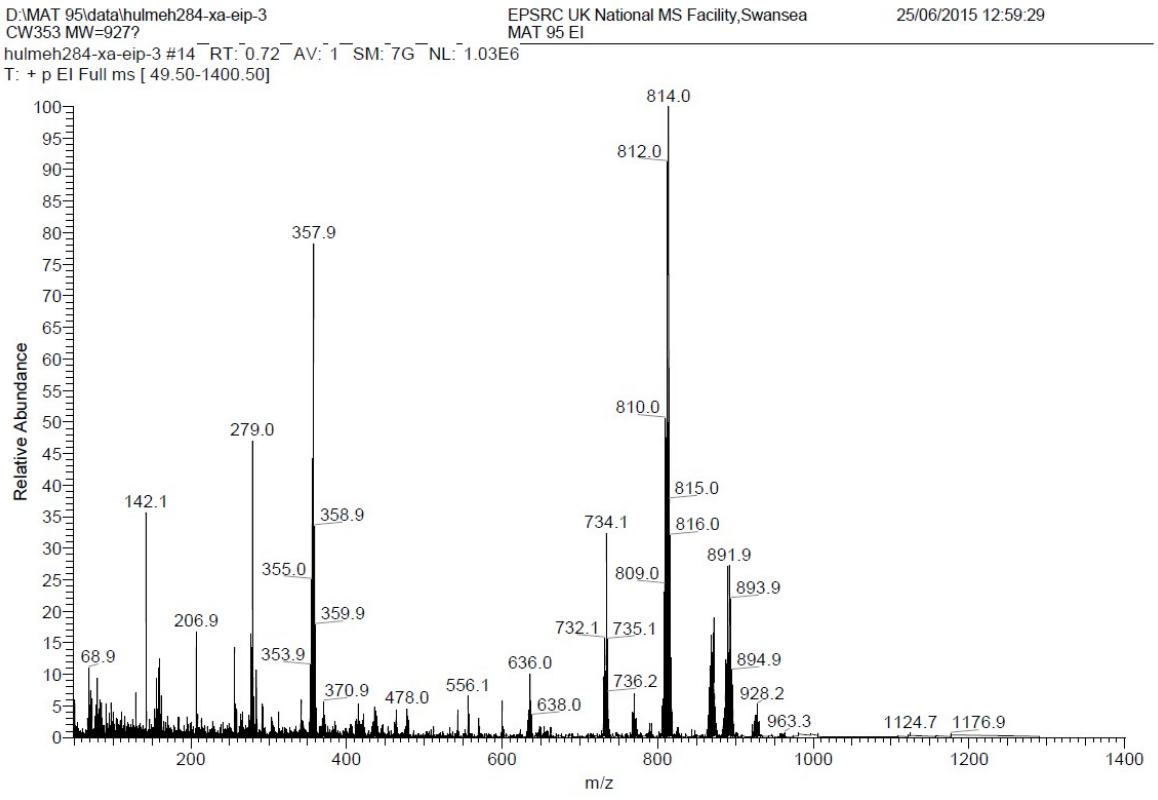

D:\MAT 95\data\hulmeh284-xa-eip-3
CW353 MW=927?

EPSRC UK National MS Facility,Swansea
MAT 95 EI

25/06/2015 12:59:29

hulmeh284-xa-eip-3 #14 RT: 0.72 AV: 1 SM: 7G NL: 8.07E5
T: + p EI Full ms [49.50-1400.50]

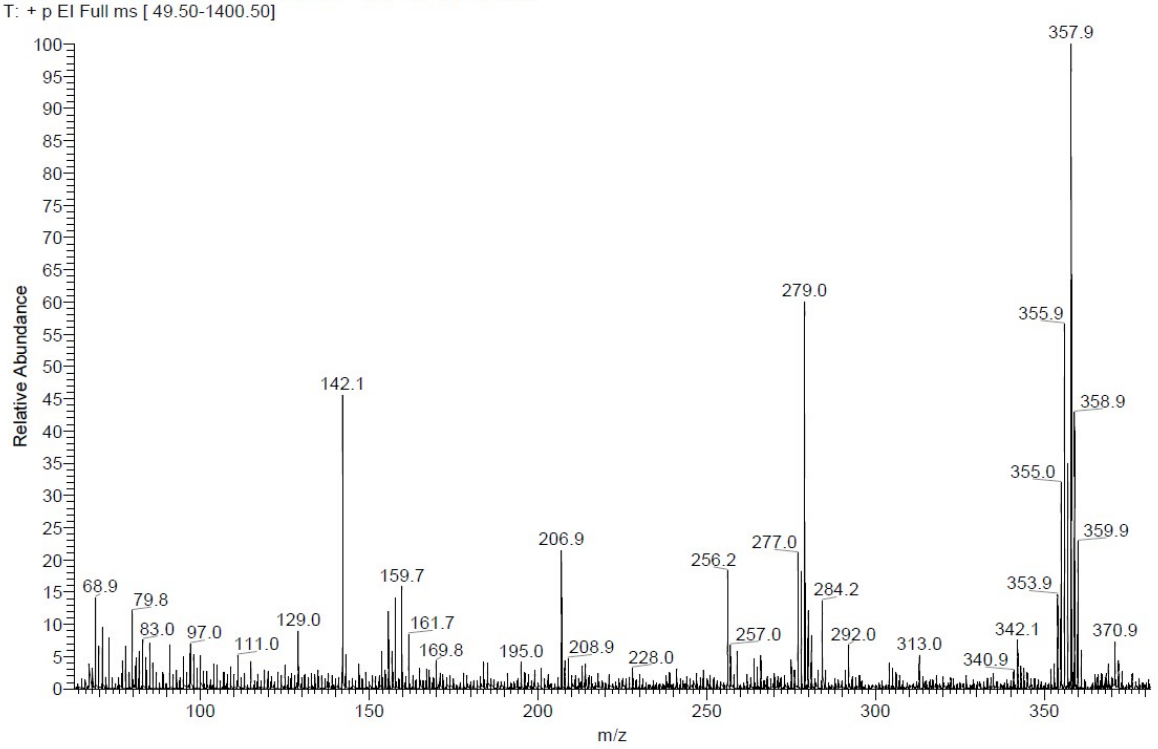

D:\MAT 95\data\hulmeh284-xa-eip-3
CW353 MW=927?

EPSRC UK National MS Facility,Swansea
MAT 95 EI

25/06/2015 12:59:29

hulmeh284-xa-eip-3 #14 RT: 0.72 AV: 1 SM: 7G NL: 1.04E5
T: + p EI Full ms [49.50-1400.50]

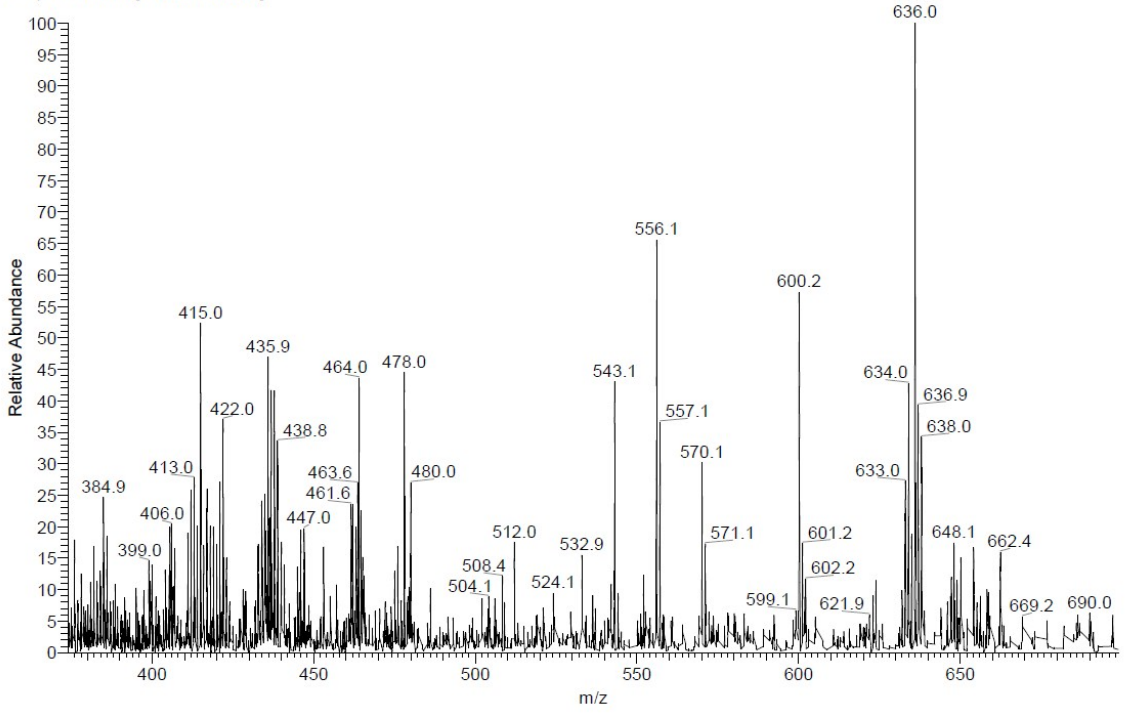

D:\MAT 95\data\hulmeh284-xa-eip-3 EPSRC UK National MS Facility,Swansea 25/06/2015 12:59:29
CW353 MW=927? MAT 95 EI
hulmeh284-xa-eip-3 #14 RT: 0.72 AV: 1 SM: 7G NL: 3.34E5
T: + p EI Full ms [49.50-1400.50]

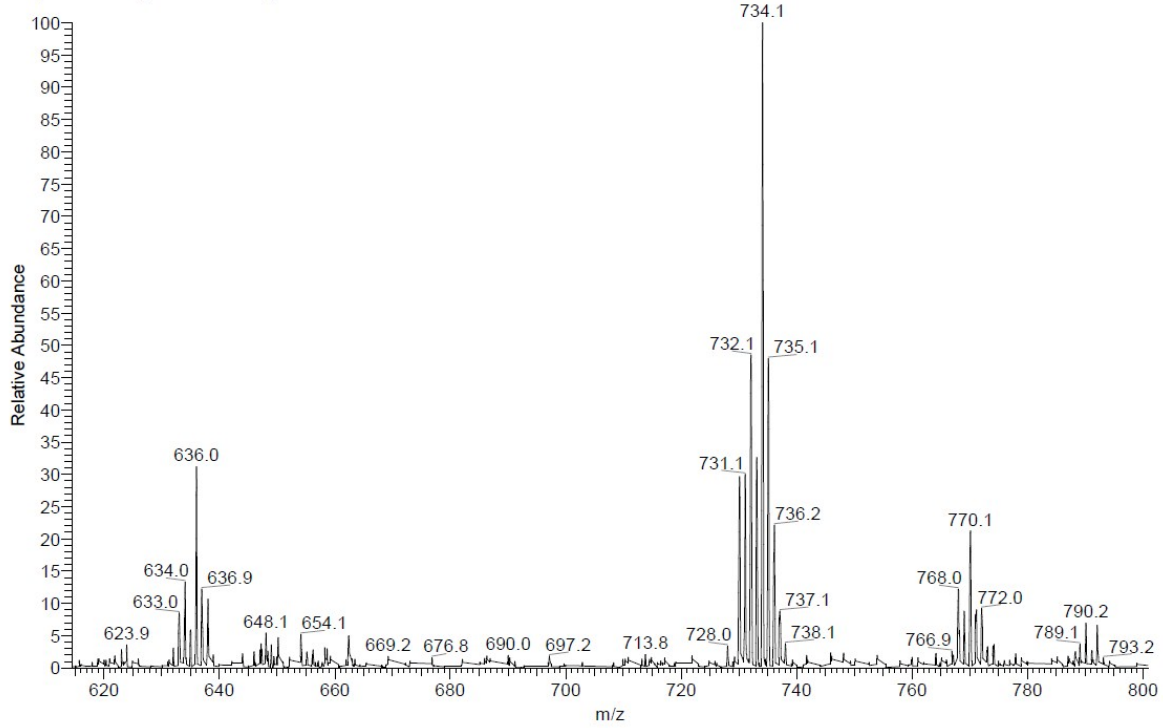

D:\MAT 95\data\hulmeh284-xa-eip-3 EPSRC UK National MS Facility,Swansea 25/06/2015 12:59:29
CW353 MW=927? MAT 95 EI
hulmeh284-xa-eip-3 #14 RT: 0.72 AV: 1 SM: 7G NL: 1.03E6
T: + p EI Full ms [49.50-1400.50]

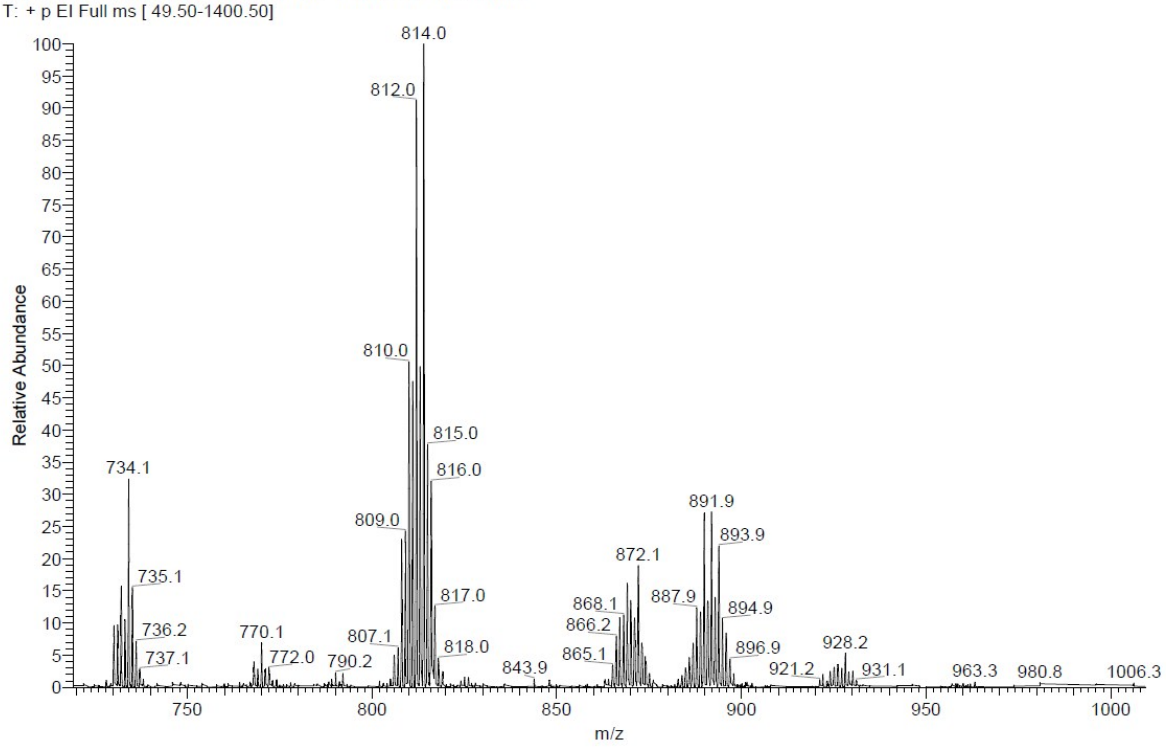

Comparison of theoretical and experimental isotope profile for compound 4

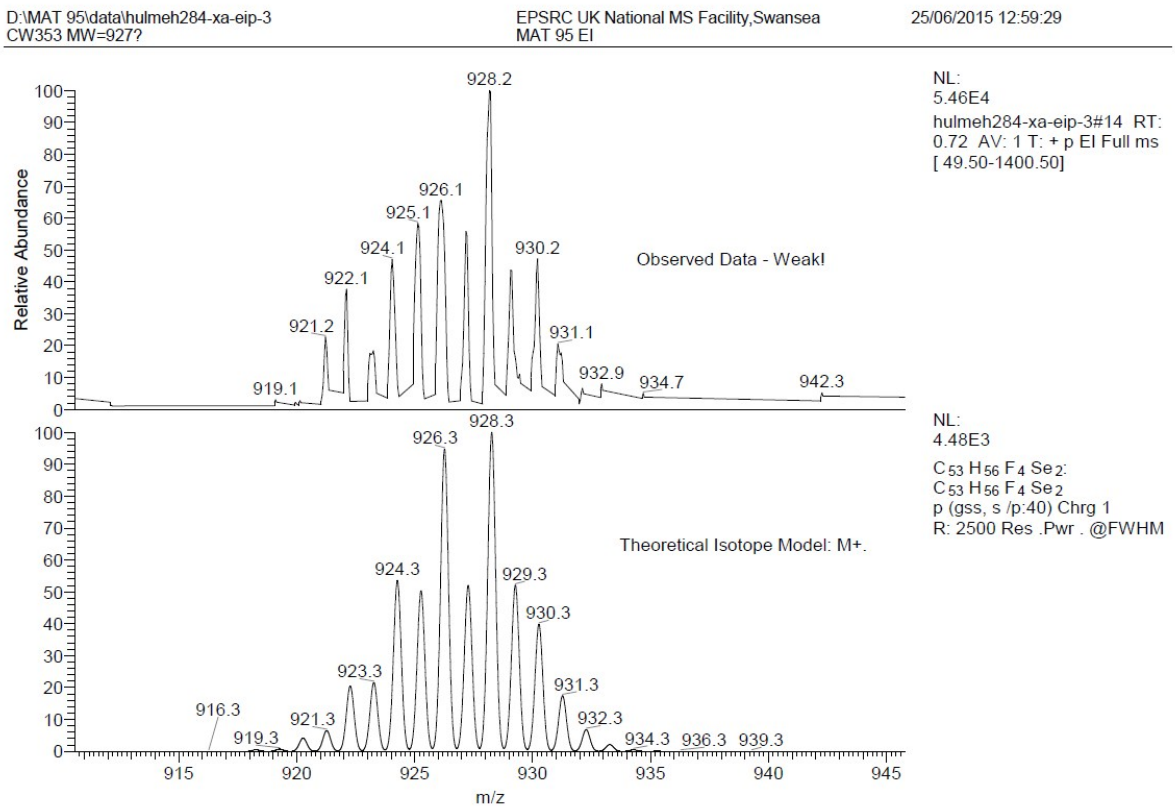

Note:

Accurate mass measurement is not possible, as the monoisotopic ions of the multiple Se multiisotopic envelope are too weak to measure accurately with current technology. Instead the isotope profile is used instead, see above. This is an issue for compounds which contain more than one Se-atom.

2.0 – Miscibility of DTC5C7 and DTSe

The miscibility of DTC5C7 and DTSe was examined under crossed polarisers using an Olympus BX50 Microscope fitted with a Mettler FP82 HT hotstage. A small amount of both samples was sandwiched between two glass plates, each 1mm in thickness.The glass cell (~1cm × 1.5cm) was heated to 160°C and compressed slightly in order to create a region of contact between the two compunds. The cell was then cooled at 10°C/min to 60°C. The key transition points (not shown in the main text) are displayed below in Figure S2.

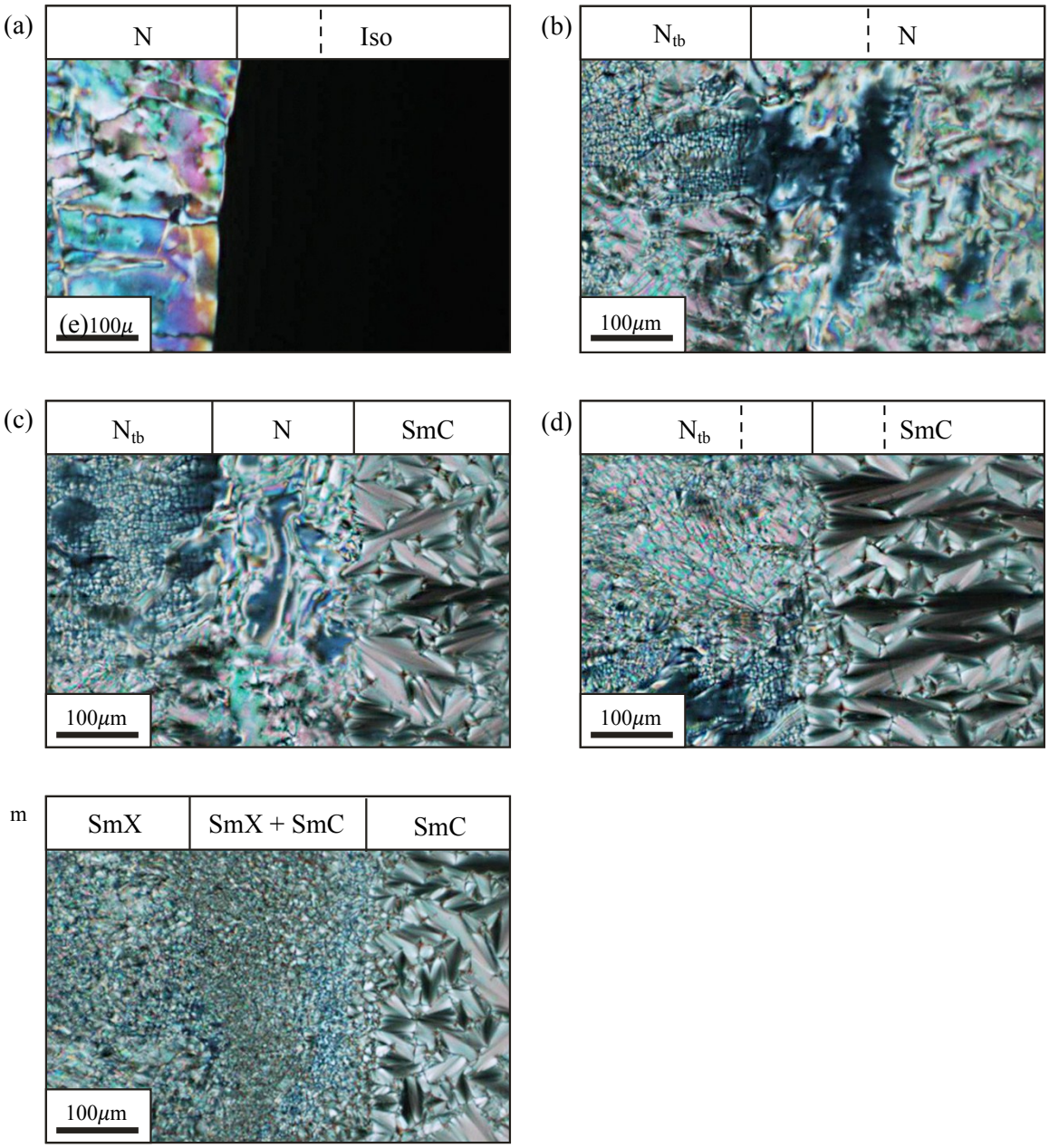

Figure S2 – The optical textures observed between crossed polarisers in a sandwich cell containing both DTC5C7 and DTSe. In all four images DTSe is on the right and DTC5C7 is on the left. The central region is a mixture of the two. Solid lines indicate phase boundaries and dashed lines indicate the approximate edge of the mixed region when it is in the same phase as one (or more) of the pure compounds. The images were taken at (a) 130°C, (b) 120°C, (c) 114°C, (d) 110°C and (e) 90°C. Iso = Isotropic, N = nematic, N_{tb} = twist bend nematic, SmC = smectic C, SmX = modulated smectic. SmX is meta-stable and only observed on cooling.

3.0 – DSC Analysis of DTC5C7, DTSe and Mixtures

The phase behaviour of all compounds and mixtures was investigated by differential scanning calorimetry (DSC) using a Perkin Elmer Diamond DSC, fitted with a ULSP liquid nitrogen cooling unit. The binary mixtures are prepared by dissolving the weighed amount of DTC5C7 and DTSe in Dichloromethane (DCM), and freeze drying after mixing in solution. The scanning rate was 10°C/min in all instances. The samples were investigated on both heating and cooling. The first heating curves are displayed below in Figure (S1) and were used to construct the phase diagram displayed in Figure 1(c) of the main text. The transition temperatures are tabulated in Table S1. The mixtures are named using the notation 'Se00', where the last two digits correspond to the molar percent of DTSe.

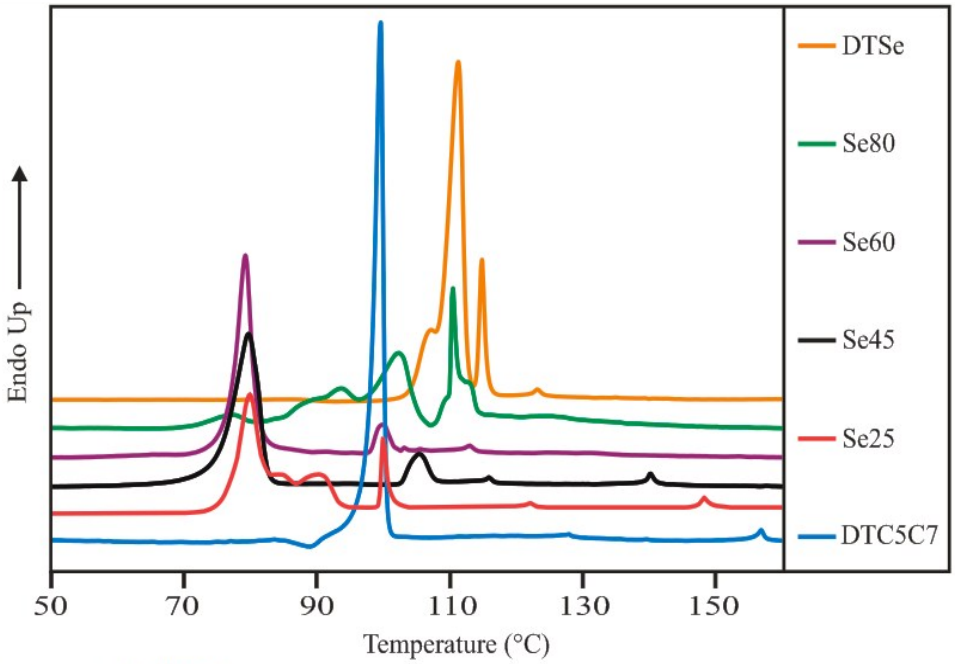

Figure S3 – First heating DSC curves of DTC5C7, DTSe and mixtures of the two compounds. The scanning rate was 10°C/min in all cases.

Table S1 – Position of temperature maxima

Sample	C → SmC (°C)	C → N_{tb} (°C)	SmC → N_{tb} (°C)	SmC → N (°C)	N_{tb} → N (°C)	N → Iso (°C)
DTC5C7	---	99.5	---	---	127.8	156.8
Se25	80	---	99.8	---	122.3	148.5
Se45	79.5	---	105.3	---	115.8	140
Se60	79	---	99.8	---	112.8	131
Se80	102.1	---	---	110.3	---	125.3
DTSe	111.2	---	---	114.8	---	123.1

The temperatures corresponding to the DSC peak positions of DTC5C7, DTSe and mixtures of both compounds. C = Crystal, SmC = Smectic C, N_{tb} = twist bend nematic, N = Nematic, Iso = Isotropic.

4.0 – X-ray Scattering of Se45

4.1 – X-ray Fluorescence of Se45

At photon energies close to the absorption (K) edge of the atom, electrons in the inner-most shells may be excited, which upon relaxation, may re-emit the absorbed photons with reduced energy. This is known as inelastic scattering or fluorescence. The fluorescence of Se45 was investigated on station I22 of the diamond light source in the energy range 12.608 – 12.708KeV, i.e. above and below the Se K-edge of 12.658KeV. Throughout the experiment the sample was held in a 1mm glass capillary. A 2D diffraction pattern was recorded in each 10eV increment of the energy range and converted to 1D by azimuthal integration. The change in background scattering, attributed to fluorescence, was determined from the baseline of the 1D diffraction patterns. These results are plotted in Figure S4 below for three different temperatures. At energies above and equal to the resonant energy, background scattering increases by a factor of ∼2.

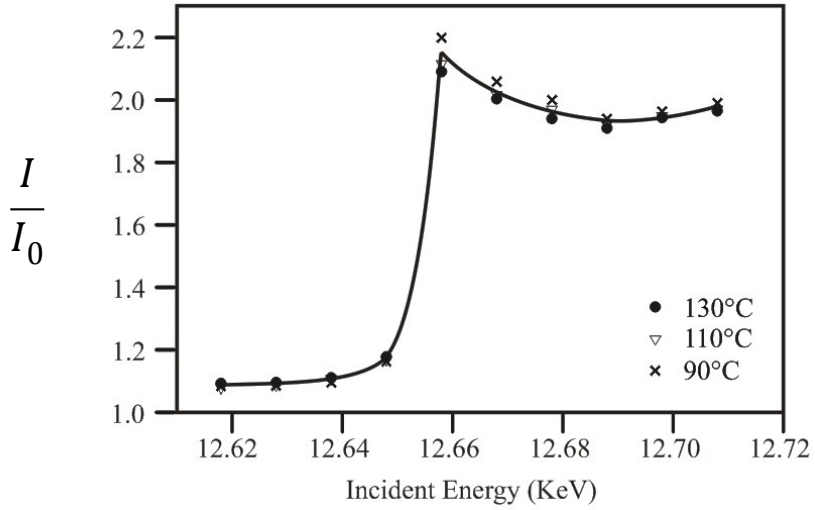

Figure S4 – The energy dependent background intensity created by fluorescent (inelastically scattered) photons in the range of q = 0.3 – 3.7nm^{-1}. The quantity I/I_0 represents the scaling factor between the initial background intensity (I_0), measured at 12.608KeV, and the background intensity measured in at each 0.01KeV increment up to 12.708KeV.

4.2 – Resonant Scattering Features of Se45

The resonant X-ray scattering (RXS) investigation of Se45 was performed on beam-line I22 of the Diamond Light Source. The sample was held in a 1 mm glass capillary. The capillary was placed in a permanently magnetised cell such that the 1T magnetic field ran perpendicular to its length. The sample was heated and cooled using nitrogen gas (Cryojet HT by Oxford Instruments). Resonance of Se45 was firstly investigated at 105°C (N_{tb} phase) in the energy range 12.608 – 12.708 keV, i.e. above and below the Se K-edge (12.658KeV). The sample to detector distance was 2.11m and the beam path was held under vacuum. Figure S5 shows 1D diffractograms recorded in each 10eV increment of the energy range. At the Se K-edge (12.658 keV) a resonant diffraction peak was observed at $q \sim 0.62$ nm^{-1}, corresponding to a d-spacing ∼10 nm.

The resonance effect was further investigated with temperature. The sample was heated and cooled using nitrogen gas (Cryojet HT by Oxford Instruments). A maximum temperature difference of 5°C was observed between nominal temperature and DSC peak position. As mentioned in the main text the resonance effect was observed only in the N_{tb} phase and at the biphasic boundaries with the neighbouring N and SmC phases. Table S2 below summarises the key observations of temperature variation on the scattering maxima observed in Se45.

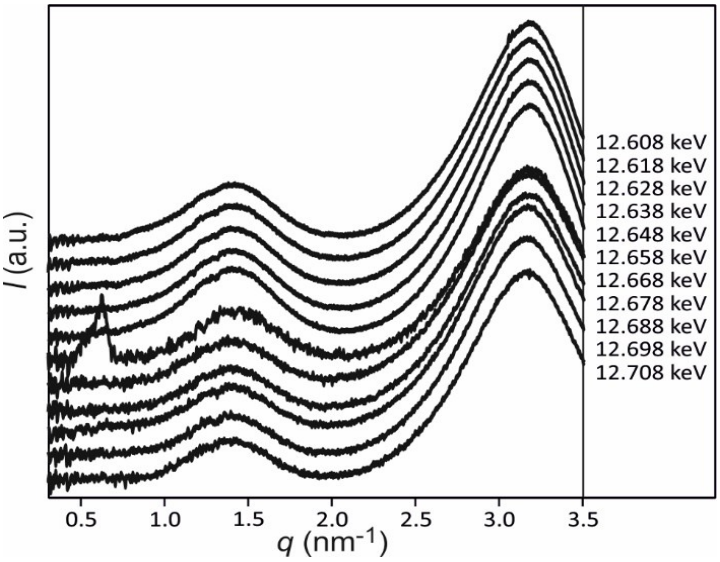

Figure S5 – The 1D diffractograms of Se45 recorded at 105°C, with incident beam energy changing from 12.608 – 12.708 keV. The resonant diffraction peak is observed at the Selenium absorption edge 12.658keV. The curves have been corrected for background scattering.

Table S2 – Summary of RXS data of Se45 during temperature scan.

	T (°C)	*p* (nm)	*d1* (nm)	*d2* (nm)	$\Delta q_{//p}$ (nm^{-1})	$\Delta q_{//d2}$ (nm^{-1})	*d3* (nm)
	120	-	4.46	2.03	-	1.28	0.46
	115	12.2	4.46	2.03	0.050	1.10	0.46
	112	12.1	4.41	2.03	0.060	1.18	0.46
	110	10.8	4.38	2.01	0.090	1.22	0.46
	107	10.4	4.36	1.99	0.075	1.18	0.46
	105	10.1	4.36	1.99	0.055	1.08	0.46
Development of SmC phase	102	9.8	4.35	1.98/2.07*	0.050	0.015	0.45
	100	9.3	4.14	2.06	0.050	0.015	0.45
	95	-	4.12	2.06	-	0.015	0.45
	90	-	4.12	2.06	-	0.015	0.45

p = helical pitch length, *d1* and *d2* respectively correspond to the average inter- and intra- molecular spacings determined from the non-resonant SAXS peaks. *d3* is the d-spacing of the WAXS peak maximum, this is related to the lateral distance between molecules, which equals to 1.117 *d3* (A. de Vries. Mol. Cryst. Liq. Cryst. **10**. 219 (1970).). The FWHM along the helical axis ($\Delta q_{//}$) of the peaks associated with *p* and *d2* are also provided. *Here the scattering maximum of the N_{tb} phase, and the Bragg reflection of the SmC phase, are simultaneously observed. The larger of the two spacings corresponds to the SmC Bragg reflection.

4.3 – Non-resonant Scattering Features of Se45

The non-resonant small and wide angle scattering (SAXS and WAXS) features of Se45 were additionally investigated on station BM28 of the European Synchrotron Radiation Facility (ESRF). The sample was investigated in both transmission and grazing incidence setups. In the transmission setup the sample was sealed in a 1.0mm diameter glass capillary and placed in a custom built heating cell. The cell was in turn placed between the poles of a superconducting solenoid, which produced a magnetic field of 3T. The magnetically aligned WAXS and SAXS diffraction patterns were collected separately using a Mar165 CCD detector. The sample to detector distance was ~30cm for the WAXS patterns and ~1m for the SAXS patterns. In both instances a helium flushed flight tube was used to reduce air scattering. The WAXS patterns are shown in

Figure 3(e-g) of the main text, while the SAXS patterns are provided below in Figure S6. Similar to the evidence provided in the main text, alignment with the field worsens with temperature, until orientation is lost entirely in the SmC phase. The SAXS peaks can also be seen to shift away from the meridian (vertical axis in S6) in the N_{tb} phase.

In the grazing incidence setup Se45 was melted onto a silicon substrate and cooled into the N_{tb} phase (110°C). The resulting thin film was then sheared to produce homeotropic alignment of the helical axis. Homeotropic alignment persisted into SmC phase, with the layer normal perpendicular to the substrate surface. This can be seen in the grazing incidence x-ray diffraction (GIXRD) patterns of the N_{tb} and SmC phases (S6). Homeotropic alignment is confirmed by the centring of the small angle peak(s) along the substrate surface normal (meridian).

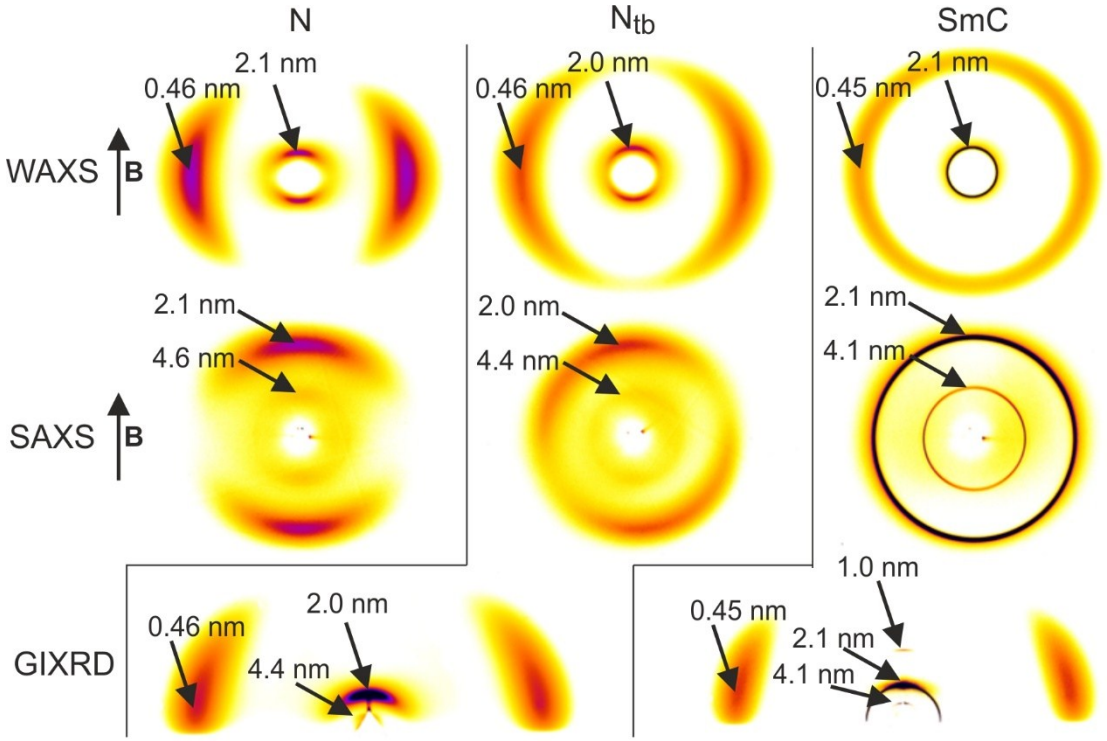

Figure S6 – Diffractograms of Se45, recorded far below the resonant energy. N: Nematic 140-116°C, N_{tb}: Twist Bend Nematic 115-106°C and SmC: Smectic-C 105-76°C.In the WAXS and SAXS patterns, the direction of the magnetic field is vertical. The GIXRD patterns show that better orientational order can be achieved in the N_{tb} and SmC phases by shearing sample.

5.0 – Geometric Calculations of the Helical Structure

Here we derive the geometric equations describing the behaviour of the molecules (assuming the ideal conformation) in the N_{tb} phase. From these equations one may estimate the average tilt angle of the mesogens and the average bend angle of the dimers, using the experimentally determined values of the pitch length (p) and average inter-mesogen height difference (h). As mentioned in the main text, p is determined from the spacing of the resonant peak (p, Table S2), while h is determined from the spacing of the outer-most non-resonant SAXS peak ($d2$, Table S2). A diagram of the molecular structure is provided below in Figure S7 to facilitate definition of the various angles and dimer components.

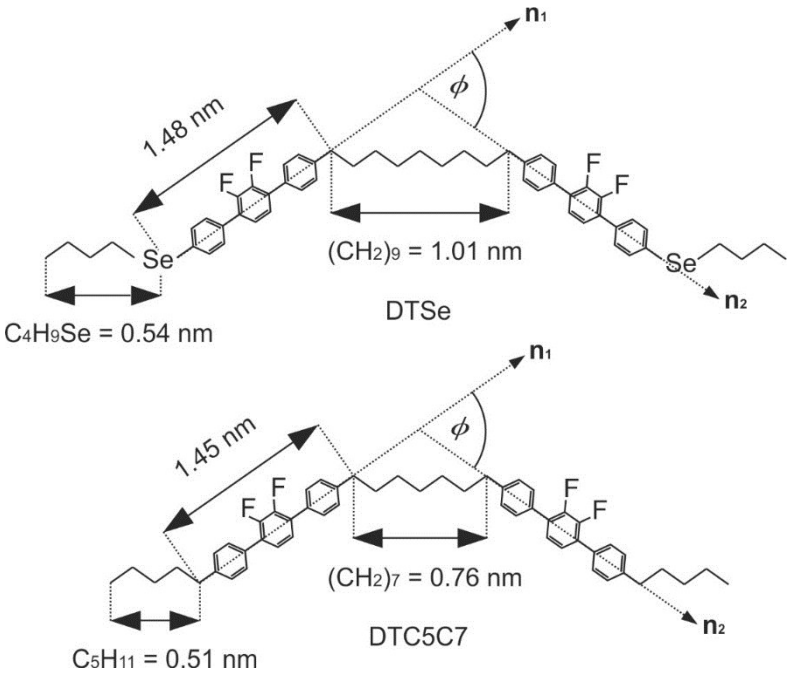

Figure S7 – Details of molecular geometry of DTSe and DTC5C7 and definition of angles and vectors. The lengths of the rigid mesogens and spacers were determined via molecular modelling using Materials Studio. The exterior bend angle ϕ and the unit vectors $\mathbf{n_1}$ and $\mathbf{n_2}$, defined here, will be referred to further below.

5.1 – Tilt Angle of the Mesogens

Firstly the value of h is linked to the helical contour length (l) between the centres of two mesogens by $h = l\cos(\theta)$. Here θ is the tilt angle between the mesogens and the helical axis $\mathbf{n_0}$. This relationship is shown diagrammatically in Figure S8 below. The average value of l in Se45 may be calculated by averaging the molecular structures of DTC5C7 and DTSe. While the lengths of different segments are shown in Figure S7, the molar average spacer length is calculated to be 0.87 nm. The average terminal chain length is 0.52 nm. The average length of the mesogen is 1.46 nm. The average contour length of the molecule is therefore calculated to be 4.75 nm. As the terminal chains tend to be conformationally more disordered, as well as partially interdigitated, the effective contour length of the molecule is expected to be shorter than that. The contour length between the two mesogens in the dimer, l, is 1.46 + 0.87 = 2.33 nm. As the value of l is assumed constant and the measured value of h is almost invariant with temperature $\simeq$ 2nm (Table S2), θ is calculated as ~29° throughout the temperature range of the N_{tb} phase.

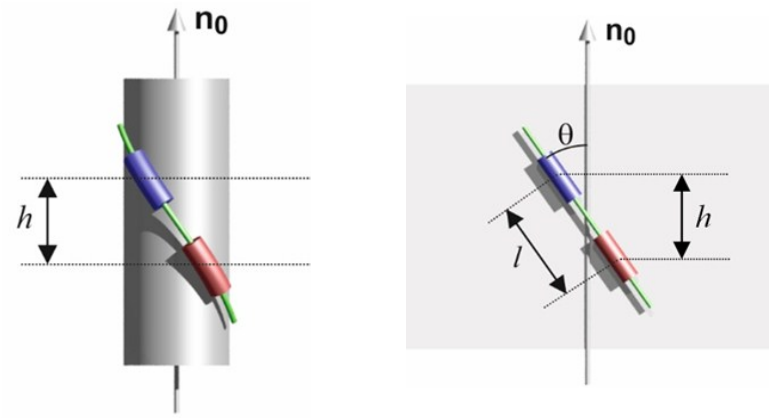

Figure S8 – Diagrammatic representation of the relationship between l, h, θ and the helical axis $\mathbf{n_0}$. On the left the molecule is wrapped around a cylinder and the distance between the two mesogens follows a helical contour. An unwrapped version of the cylinder is shown on the right. Here the molecule is straight (mesogens parallel with $\phi = 0$).

5.2 - BendAngle of the Dimers

As mentioned in the main text, on progression along $\mathbf{n_0}$ each mesogen is rotated about the helical axis by an angle of $2\pi h/p$ in respect to the previous one. Here this rotation angle will be denoted by α. If each of the two rod-like mesogens of a dimer are respectively assigned unit vectors $\mathbf{n_1}$ and $\mathbf{n_2}$, the exterior angle between them (ϕ) can be written:

$$\sin\frac{\phi}{2} = \sin\theta\sin\frac{\alpha}{2} = \sin\theta\sin\left(\frac{\pi h}{p}\right) \qquad (Eqn.\ S1)$$

Here, ϕ is the bend angle of the dimers as defined in Figure S7. As sin(θ) is approximately constant in the N_{tb} phase, the bend angle is dependent only on the rotation angle α (Figure S9), which in turn is dependent on the pitch length *p*. As shown in Table S2, *p* ranges between 9 and 12nm. Using equation S1 we calculate that the value of ϕ increases on cooling, from 28° (115°C) to 35° (105°C).

5.3 – Twist Angle of the Dimers

For the dimer molecules another important parameter to describe its shape is its twisting angle, i.e. the angle between the two mesogens when projected along the spacer axis (for an all-trans spacer the twisting angle is 0, Figure 4a main text). The twisting angle can be calculated using the directors of the two mesogens, and that of the spacer in the middle. Taking the vertical position of the spacer as reference (*z*=0), the heights of the two mesogens are ±*h*/2 respectively. Therefore the director of the spacer

$$\mathbf{n}_s = \sin\theta\,\boldsymbol{i} + \cos\theta\,\boldsymbol{k} \qquad (Eqn.\ S2a)$$

and the directors of the two mesogens

$$\mathbf{n}_1 = \sin\theta\cos(-\pi h/p)\boldsymbol{i} + \sin\theta\sin(-\pi h/p)\,\boldsymbol{j} + \cos\theta\,\boldsymbol{k} \qquad (Eqn.\ S2b)$$

$$\mathbf{n}_2 = \sin\theta\cos(\pi h/p)\boldsymbol{i} + \sin\theta\sin(\pi h/p)\,\boldsymbol{j} + \cos\theta\,\boldsymbol{k} \qquad (Eqn.\ S2c)$$

Therefore we have $(Eqn.\ S3)$

$$\mathbf{n}_1 = (\sin^2\theta\cos(\pi h/p) + \cos^2\theta)\mathbf{n}_s - 2\sin\theta\cos^2\theta\sin^2(\pi h/2p)\,\boldsymbol{i} - \sin\theta\sin(\pi h/p)\,\boldsymbol{j} + 2\sin^2\theta\sin^2(\pi h/2p)\cos\theta\,\boldsymbol{k}$$

$$\mathbf{n}_2 = (\sin^2\theta\cos(\pi h/p) + \cos^2\theta)\mathbf{n}_s - 2\sin\theta\cos^2\theta\sin^2(\pi h/2p)\,\boldsymbol{i} + \sin\theta\sin(\pi h/p)\,\boldsymbol{j} + 2\sin^2\theta\sin^2(\pi h/2p)\cos\theta\,\boldsymbol{k}$$

The twist angle δ

$$\cos\delta = \frac{\cos^2\theta\sin^2\left(\frac{\pi h}{2p}\right) - \sin^2\theta\cos^2\left(\frac{\pi h}{2p}\right)}{\cos^2\theta\sin^2\left(\frac{\pi h}{2p}\right) + \sin^2\theta\cos^2\left(\frac{\pi h}{2p}\right)} \qquad (Eqn.\ S4)$$

According to equation S4 the twisting angle can be calculated to be 129° at 115°C, and 125° at 105°C.

5.4 – Tilt Angle of the Dimers

An additional quantity, not discussed in the main text, is the effective tilt angle of the dimers in respect to the helical axis. The direction of a dimer is defined as the vector connecting the centres of the two mesogens of the dimer, and the dimer tilt angle β is the angle of this vector towards the helical axis. Where the symbols have their previously defined meanings, the radius r of the cylinder (hence the helix) can be defined from simple helical geometry as (Figure S9):

$$r = \frac{p\tan\theta}{2\pi} \qquad (Eqn.\ S5)$$

We may also define a chord length w (Figure S9), which represents the projected distance between two mesogens in the plane perpendicular to $\mathbf{n_0}$.

$$w = 2r\sin\left(\frac{\alpha}{2}\right) = \frac{p\tan\theta}{\pi}\sin\left(\frac{\alpha}{2}\right) \qquad (Eqn.\ S6)$$

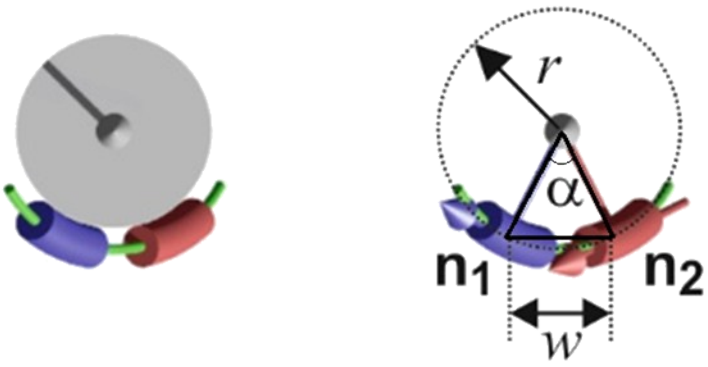

Figure S9 – Diagrammatic representation of the rotation angle between successive mesogens (α), the unit vectors $\mathbf{n_1}$ and $\mathbf{n_2}$, the radius of the helix (r) and the projected chord length w.

The tilt angle of the dimers β, in respect to the helical axis can then be defined from simple geometry as:

$$\tan\beta = \frac{w}{\mathrm{h}} = \tan\theta\frac{\sin\left(\frac{\alpha}{2}\right)}{\alpha/2} \qquad (Eqn.\ S7)$$

The tilt angle β as a function of the mesogen tilt angle and pitch is listed in Table S3.

Table S3 – The dimer tilt angle β as a function of the mesogen tilt angle θ and helical pitch p.

$\theta \backslash p$	9 nm	10 nm	11 nm	12 nm
20°	18.00°	18.37°	18.65°	18.86°

25°	22.60°	23.05°	23.38°	23.64°
30°	27.26°	27.78°	28.16°	28.45°
35°	32.00°	32.57°	32.99°	33.31°
40°	36.83°	37.44°	37.88°	38.22°
45°	41.75°	42.38°	42.84°	43.19°

6.0 – Molecular Modelling

Molecular modelling was carried out in order to show how a smaller bend angle (ϕ), between the two mesogenic arms of a dimer molecule, can be achieved by changing of the C-C torsion angles in the spacer. We have also estimated the energy cost associated with such changes of torsion angles in the spacer.

The modelling of the molecules was carried out using Materials Studio (BIOVIA). In the modelling, the conformations of the (-C_7H_{14}-) spacer are studied, starting from the all-trans conformation where all six torsion angles in the spacer are $\gamma = 180°$. Assuming that the spacer is always helical, the six torsion angles are kept to the same value γ, changing from 180° to 150° with 5° steps. The bend angle ϕ is measured for each torsion γ (Figure S10) and listed in Table S4. The energies of the spacer in different conformations are calculated, using Universal Forcefield, and compared in Table S5. According to Table S5, the ideal torsion angle γ should be around 160° as the experimentally measured bend angle ϕ from X-ray studies is around 29°. For the same molecular conformation, the twist angle δ of the dimer is measured to be 128° (Figure S10c), which corresponds remarkably well with the experimentally determined values of between 129° and 125° as shown in section 5.3. Even though the energy involved in such a conformational change from the all-trans state seems to be high, ~5.8 kcal/mol, it is an over-estimation as the many other spacer conformations that achieve the same bend angle were not explored. A high energy conformational state can in fact be stabilized by the high entropy of the spacer, i.e. the various different conformations the spacer can take.

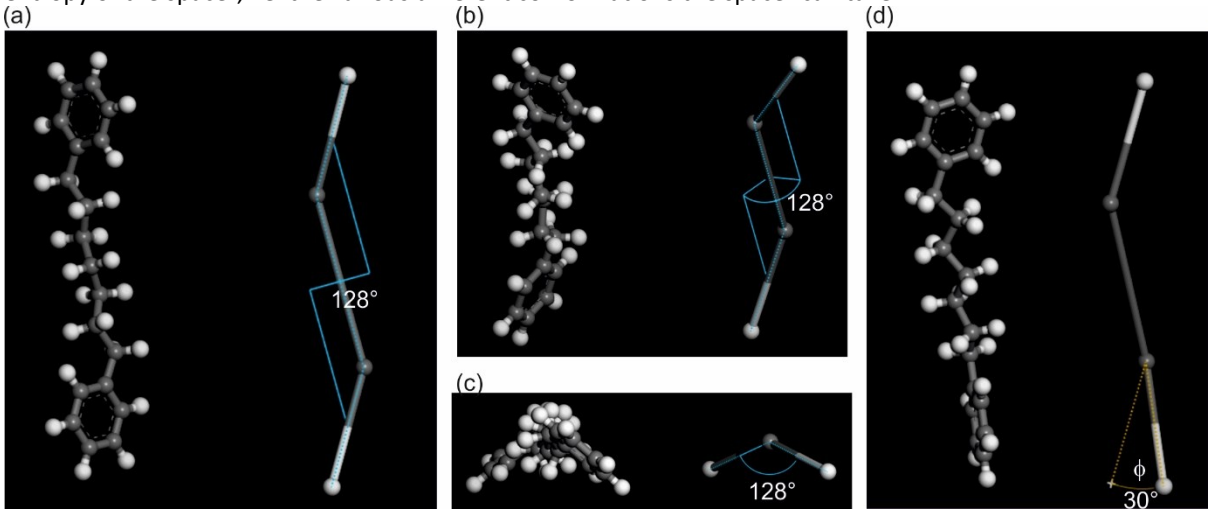

Figure S10. The molecular model of DTC7 with torsion angles in the spacer $\gamma = 160°$. For simplicity only the spacer and the two phenyl rings directly connected to the spacer are shown. To show the molecular geometry more clearly a rod model of the molecule is shown on the right hand side, where the C-C bond represents the spacer, and C-H bonds the mesogens. (a-c) The twist angle δ of the two mesogens around the spacer is measured to be 128°: (a) view when the spacer is parallel to the paper; (b) tilted view, (c) view along the spacer. (d) The bend angle ϕ of the dimer, i.e. the angle between the two mesogens, is measured to be 30°.

Table S4. The bend angle ϕ of a dimer as a function of torsion angles γ adopted by the spacer.

γ(°)	ϕ(°)
180	56.1
175	54.0

170	48.4
165	39.3
160	29.6
155	14.9
150	1.4

Table S5. Energy estimation of spacer (-C_7H_{14}-) with different torsion angles γ.

γ(°)	Total (kcal/mol)	Valence (kcal/mol)	Non-Bond (kcal/mol)
180	3.997	1.248	2.750
175	4.359	1.463	2.896
170	5.444	2.096	3.348
165	7.250	3.106	4.144
160	9.755	4.423	5.332
155	12.941	5.952	6.989
150	16.880	7.604	9.276